Journal of Iberian Geology (2020) 46:369–402
https://doi.org/10.1007/s41513-020-00139-8

RESEARCH PAPER

Three-dimensional analysis of the titanosaurian limb skeleton: implications for systematic analysis

Adrián Páramo[1] · **Pedro Mocho**[1,2] · **Francisco Ortega**[1]

Received: 2 March 2020 / Accepted: 15 September 2020 / Published online: 13 October 2020

Abstract

The titanosaurian appendicular skeleton exhibits morphological similarities among different clades and its osteological information is usually less taxonomically meaningful than those of other regions of the skeleton. There is a probable morphological convergence due to morphofunctional similarities between members of different titanosaurian groups. In addition, higher intraspecific variability has hindered the assessment of similar forms such as the Late Cretaceous titanosaurians of the Ibero-Armorican domain. The use of 3D-geometric morphometrics and discriminant analyses on an abundant sample of titanosaurian limb elements from the Lo Hueco site and other titanosaurian taxa has been able to characterize the differences between several sauropod clades with the control of the intraspecific variability. Similar methods with the use of surface analyses of other titanosaurs enabled the recognition of morphological similarities congruent with morphofunctional convergences between one of the lithostrotian morphotypes identified in Lo Hueco (the Morphotype II) and some gracile colossosaurs such as *Mendozasaurus neguyelap*. In contrast, Morphotype I at Lo Hueco present a more typical titanosaurian morphology, resembling *Jainosaurus* cf. *septentrionalis*. The use of discriminant analyses allowed us to distinguish Colossosauria on the basis of limb morphology for the first time. We also observed that Colossosauria and Saltasauridae diverge from a more typical titanosaurian non-autopodial limb skeleton. Our results also suggest a highly different and specialized limb skeleton for the Saltasauridae in comparison with other sampled titanosaurians. The use of surface semilandmarks and discriminant analyses also allowed us to propose several new potential osteological characters for use in phylogenetic analyses through the maximization of differences between the sampled clades.

Keywords Titanosauria · Lo Hueco · Geometric morphometrics · Cretaceous · High density surface semilandmarks

Resumen

El esqueleto apendicular de los titanosaurios presenta similitudes morfológicas entre clados muy diversos y su información osteológica es de menor utilidad para taxonomía respecto a otras regiones del esqueleto. Es possible que se produzca una convergencia morfológica debido a similitudes morfofuncionales entre miembros de los diferentes grupos de titanosaurios. Además, la elevada variabilidad intraespecífica ha dificultado la diferenciación entre formas de titanosaurio morfológicamente similares en el Cretácico tardío del dominio Ibero-Armoricano. El uso de técnicas de morfometría geométrica 3D así como análisis discriminante en una muestra abundante de ejemplares apendiculares del yacimiento de Lo Hueco y otros taxones de titanosaurio ha permitido caracterizar algunas diferencias entre los distintos clados de titanosaurios con el control de la variabilidad intraespecífica. Estos métodos se aplicaron también en análisis de superficies permitiendo reconocer similitudes morfológicas congruentes con convergencias morfofuncionales entre uno de los morfotipos de lithostrotios identificados en

Electronic supplementary material The online version of this article (https://doi.org/10.1007/s41513-020-00139-8) contains supplementary material, which is available to authorized users.

✉ Adrián Páramo
paramoblazquez@gmail.com

[1] Grupo de Biología Evolutiva (Ref. GI314), Departamento de Física Matemática y Fluidos, Facultad de Ciencias, Universidad Nacional de Educación a Distancia, Madrid, Spain

[2] Instituto Dom Luiz, Faculdade de Ciências da Universidade de Lisboa, Lisbon, Portugal

Lo Hueco (Morfortipo II) y formas gráciles de colossosaurios como *Mendozasaurus neguyelap*. Sin embargo, el Morfotipo I de Lo Hueco presentaría una morfología titanosauriana más típica, asemejándose a *Jainosaurus* cf. *septentrionalis*. El uso de análisis discriminantes permitió distinguir Colossosauria en base a la morfología de sus extremidades por primera vez. También se puede observar que la morfología de Colossosauria y Saltasauridae divergen de morfologías apendicular no autopodiales más típicamente titanosaurianas. Nuestros resultados sugieren que las grandes diferencias morfológicas de las extremidades de Saltasauridae con otros clados se debería a su especialización en comparación a otros titanosaurios muestrados en este estudio. El uso de semilandmarks de superficie y análisis discriminante permitió proponer una serie de potenciales caracteres osteológicos nuevos, útiles para el análisis filogenético, gracias a maximizar las diferencias existentes entre los diferentes clados muestreados.

Palabras clave Titanosauria · Lo Hueco · Morfometría Geométrica · Cretácico · Semilandmarks de superficie de alta densidad

1 Introduction

The titanosaurian appendicular skeleton has been poorly known until the last few decades, even though the study of this region of the skeleton is critical in several events in the evolutionary history of the neosauropod bauplan and posture (Carrano 1998, 2005; Wilson and Carrano 1999; Apesteguía 2005; Henderson 2006; Bates et al. 2016; González Riga et al. 2019). In addition, the appendicular skeleton bears osteological information used in morphological datasets for sauropod phylogenetic analyses (e.g. Salgado et al. 1997; Wilson 2002; Upchurch et al. 2004; Mannion et al. 2013; Carballido et al. 2012, 2017; González Riga et al. 2019). However, many studies of sauropod cladistics have lacked information on numerous titanosaurian taxa until recently, caused by the fragmentary record of those taxa (e.g. Wilson and Upchurch 2003; Bonnan 2004; Upchurch et al. 2004; Ullmann et al. 2017; González Riga et al. 2019). Until the mid-to-late 1990 most of the best known titanosaurians were from derived lithostrotian taxa, so this lack of information produced a bias in the osteological information toward these derived forms (González Riga et al. 2019). Most of the osteological information and the best known titanosaurians were primarily taxa referable to Saltasauridae, a deeply nested clade with a specialized appendicular structure (see Powell 1992, 2003; Carrano 2005; Bates et al. 2016; Ullmann et al. 2017; Otero 2018; González Riga et al. 2019). The saltasaurid sauropods possessed a massive and robust appendicular skeleton configured into a unique stance termed "wide-gauge" posture (e.g. *Opisthocoelicaudia skarzyinski* Borsuk-Bialynicka 1977; *Saltasaurus loricatus* Powell 1992, 2003; *Neuquensaurus australis* Lydekker 1893; Otero 2010). Recent discoveries of new titanosaurian material highlight a wider degree of morphological differences in the derived titanosauriform skeleton, and analysis of these new materials could help to assess the phylogenetic affinities among the more inclusive groups (González Riga et al. 2019). Moreover, phylogenetic affinities of several of these titanosaurian subclades are still debated, as additional information of new taxa allow several already known titanosaurs to be reassessed. This new osteological information and recent discoveries sometimes results in relocation of several already known titanosaurian forms in other previously known inclusive groups within Titanosauria (González Riga et al. 2018; Mannion et al. 2019) or else the proposal of entirely new exclusive clades within Titanosauria (e.g. Lirainosaurinae Díez Díaz et al. 2018a, b).

In addition, the lack of complete specimens of earlier branching non-saltasaurid titanosaurs complicates the description and assessment of osteological characters. This is especially relevant for the appendicular skeleton (González Riga et al. 2019) as osteological characters from this region are sometimes convergent among titanosauriforms or between titanosauriforms and non-titanosauriforms (see comments in the Character list in Tschopp et al. 2015) Therefore, because of these morphological similarities many of the osteological features are not taxonomically meaningful (see Wilson and Upchurch 2003; Vila et al. 2012).

In this context, the Late Cretaceous in the Ibero-Armorican domain has yielded many titanosaurians: *Ampelosaurus atacis* Le Loeuff 1995, *Lirainosaurus astibiae* Sanz et al. 1999, *Atsinganosaurus velauciensis* Garcia et al. 2010 and *Lohuecotitan pandafilandi* Díez Díaz et al. 2016 as well as some still undescribed titanosaurian forms (Canudo et al. 2001; Vila et al. 2012; Ortega et al. 2015; Díez Díaz et al 2018a, b). There is also an abundant sample of appendicular material retrieved from the known Ibero-Armorican titanosaurian localities (see localaties of *Ampelosaurus atacis* Le Loeuff 1995 2005; locality of *Lirainosaurus astibiae* Sanz et al. 1999; Pereda Suberbiola et al. 2000, 2015; Díez Díaz et al. 2015; and locality of *Lohuecotitan pandafilandi* Díez Díaz et al. 2016 Ortega et al. 2015; see also the Campanian–Maastrichtian of Chera locality in Company et al. 2009, Díez Díaz et al. 2015; and the early and late Maastrichtian south Pyreneab localities in Vila et al. 2012). Taxonomical assessment of several of these undescribed forms have been difficult in the past because of the lack of morphological

taxonomically meaningful features in the appendicular skeleton, which also make it difficult to assess the taxonomical diversity and the cladistic relationships of those taxa within the referred bonebeds. Recent studies on the limb skeleton of Late Cretaceous Ibero-Armorican lithostrotians have tried to identify osteological features that can be useful to differentiate among described and still undescribed titanosaurian forms, specifically those that could be related to autapomorphic features (e.g. *linea intermuscularis cranialis* or relative development of the trochanteric shelf of the femur, Vila et al. 2012) but the morphological variability within the Ibero-Armorican titanosaurs is greater than previously reported (e.g. *linea intermuscularis cranialis* present in both fermoal morphotypes at Lo Hueco Páramo et al. 2016, 2018; differences in the robustness of different morphotypes within the same fossil site Díez Díaz et al. 2015). Moreover, the implications of the taxonomical assessment and the identification of potential new characters could help to recognize common features among these taxa and other titanosaurian forms, and whether some osteological characters are found in more exclusive groups or are more widespread among different subclades (i.e. discussion about the femoral *linea intermuscularis cranialis* in Vila et al. 2012). Identifying putative synapomorphic features is important as recent phylogenetic hypotheses debate the presence of an endemic titanosaurian group in the Ibero-Armorican domain during the Late Cretaceous and its phylogenetic relationships with other Late Cretaceous titanosaurian faunas, especially the ones from East Europe and North Africa (Díez Díaz et al. 2018a, b; Mocho et al. 2019a). The sample of titanosaurs from the Konzentrat-Lagerstätten at Lo Hueco has yielded numerous axial and appendicular elements in different states of preservation and is proving to be relevant in this analysis (Fig. 1; see Ortega et al. 2015; Díez Díaz et al. 2016). This unique and abundant sample has allowed the assessment of morphological features relatable to taxonomic differences between two main morphotypes of appendicular elements (Páramo et al. 2017a). The use of Geometric Morphometrics toolkit (GMM) enabled us to assess the more probable number of morphotypes in the sample and allocate the isolated specimens. The specimens of Morphotype I are closely related with the holotype of *Lohuecotitan pandafilandi* (Mocho et al. 2019a; Páramo et al. 2019). Following the association of the elements from Diez Diaz et al. (2016) as well as the associated individuals HUE-EC-05 (ulna HUE-964, femur HUE-1366), HUE-EC-11 (humerus HUE-817, femur HUE-930) and a forelimb zeugopodium (ulna HUE-1139, radius HUE-1140) we can refer all the elements of Morphotype I (including *L. pandafilandi*) as very close forms if not the same taxon based on the quite robust limb skeleton, a shorter humerus with the typical hourglass morphology, ulnae with a markedly wide anteromedial and olecranon processes, femora with globous femoral head and distal end, low eccentricity of the shaft and a pronounced *linea intermuscularis cranialis*, a robust tibia with marked secondary cnemial crest and fibula with autapomorphic medially deflected anterior crest and square-shaped proximal. It is important to note that these common features have been identified after our analyses (e.g. Páramo et al. 2019) assessing several partially articulated individuals, as the *Lohuecotitan pandafilandi* holotype specimen does not preserve the humerus and radius. A second morphotype, Morphotype II, refers to a different titanosaur with more gracile and columnar appendicular elements. Given the association of the individual HUE-EC-13 (humerus HUE-1647, femur HUE-1183) and a hindlimb zeugopodium (tibia and fibula HUE-1612) it is plausible that this entire cluster can refer to the same morphotype and all the elements pertain to the same taxa. They share a more elongated and plesiomorphic humeri with slightly quadrangular proximal, extremely gracile ulnae, columnar femora with anteroposterior compression along the whole shaft, and extremely gracile tibiae which generally exhibit a secondary trochanter in the fibular articulation. We believe that the morphological differences recognized are probably taxonomically and phylogenetically significant, following previous attempts to recognize different morphotypes or morphospecies in the Ibero-Armorican domain (e.g. Vila et al. 2012; Díez Díaz et al. 2015; Mocho et al. 2018). However, the presence of more than one titanosaur form among the elements of each morphotype should not be disregarded (see Ortega et al. 2015; Páramo et al. 2017a; also, the problem of whether these morphological features are taxonomically meaningful as commented above). Regardless of the taxonomic status, both morphotypes come from different taxonomic units referable to Lithostrotia (Díez Díaz et al. 2016; Mocho et al. 2019b, c). Morphotype II includes elements from at least one taxonomic unit different from *L. pandafilandi* and other known Ibero-Armorican titanosaurian forms, and present features that allow its inclusion within Lithostrotia (e.g. all radii reported from Lo Hueco present a proximolateral bevelling, Curry Rogers 2005; posterolateral bulge on the humerus, Carballido et al. 2017; and dorsally deflected femoral head over greater trochanter of the femur, Poropat et al., 2016). In addition, the analyses of several specimens belonging to the axial skeleton have allowed the identification of multiple morphotypes (at least three) and suggest that Lo Hueco titanosaurs are all members of Lithostrotian (Mocho et al. 2016, 2019b). The GMM analyses allowed the assessment of the intraspecific variability in each morphotype and characterization of the areas that present most of the morphological variance between the two forms.

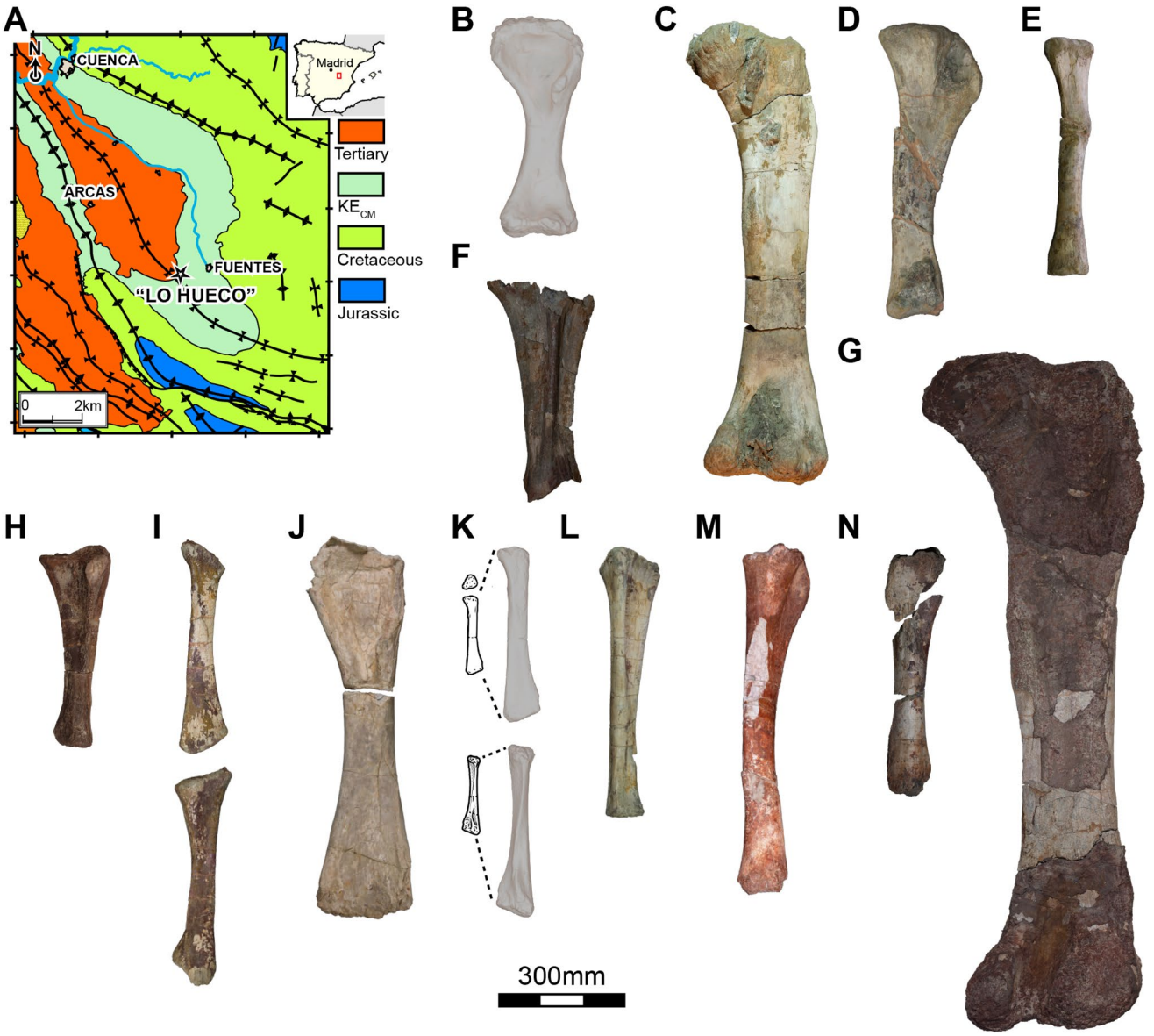

Fig. 1 Titanosaurian stylopodial elements. Location and chronostratigraphic context of the Lo Hueco fossil site (**a**), Morphotype I from Lo Hueco: left humerus 3D mesh representation of HUE-817 in anterior view (**b**); *Lohuecotitan pandafilandi* right hindlimb: femur HUE-3108 in posterior view (**c**), tibia HUE-3082 in lateral view (**d**) and fibula HUE-3087 in lateral view (**e**), *L. pandafilandi* left ulna HUE-3044 in anterior view (**f**); Morphotype II right femur HUE 594 in posterior view (**g**); Morphotype I associated left ulna HUE-1139 (**h**) and left radius HUE-1140 in anterior view (**i**). Morphotype II from Lo Hueco: left humerus HUE-1434 in anterior view (**j**), left radius 3D mesh representation of HUE-1166 in posterior view (**k**), right ulna HUE-1158 in anterior view (**l**), right tibia HUE-2117 in lateral view (**m**), left fibula HUE-1146 in lateral view (**n**). Scale bar for **a** indicated in the inset; scale for all other figures as indicated beneath the bone images

The difficulties related to the taxonomic assessment and description of potential osteological characters in titanosaurs appendicular elements is also related to the presence of morphological similarities between distinct titanosauriform groups (Ullmann et al. 2017). The appendicular skeleton of phylogenetically distant groups commonly presents morphological convergence given the current phylogenetic hypotheses, which is probably due to the presence of morphofunctional similarities among those groups (Henderson 2006; Ullmann et al. 2017). In order to assess the morphological differences between these groups, the analysis should take into account this aforementioned probable convergence among the sampled titanosaurs. The use of GMM can help to study these differences, analyse the possible convergence, and ultimately identify the areas of the non-autopodial skeleton that can be helpful for sauropod

cladistic analyses. The unique sample of Ibero-Armorican titanosaurs is an opportunity to analyse this morphological variability, identify, and codify potential useful characters for cladistics analyses. The Ibero-Armorican lithostrotian record represents a diverse sample and they exhibit morphological features that were previously thought as exclusive to other non-European titanosaurian clades (e.g. the *linea intermuscularis cranialis* of the femur mentioned above, Vila et al. 2012; the secondary cnemial crest of the tibia, Ullmann and Lacovara, 2016). The improvement on data matrices used for cladistic analyses are important in order to revaluate the still poorly known evolutionary history within exclusive faunas Ibero-Armorican titanosaurian taxa, *Atsinganosaurus velauciensis*, *Ampelosaurus atacis*, *Lirainosaurus astibiae*, and *Lohuecotitan pandafilandi*. The sample of appendicular elements found in Lo Hueco site and the referred material of *Lirainosaurus astibiae* from the Laño site (previously compared in Páramo et al. 2017a) represent a diverse sample to start assessing this morphological variation. A similar workflow can be replicated in order to include other taxa from the titanosaurian record and compare, with a control of the within-group variance and the variance between the different titanosaurian groups. GMM is also able to exclude size-dependent effects from the shape analyses like presence of putative juvenile individuals among the sampled specimens and differences between giant titanosaurian taxa (e.g. *Argentinosaurus huinculensis*) with representative of smaller titanosaurs (e.g. *Lirainosaurus astibiae*, *Rinconsaurus caudamirus* and *Saltasaurus loricatus*). This allows the observation of probable morphological convergence in the appendicular skeleton among more inclusive titanosaurian groups. The GMM tool-kit can also be used to analyse the morphological variation that is relatable exclusively to differences between said titanosaurian clades, and therefore discuss their implications with actual osteological character definitions or help to assess potential new character definitions.

2 Methodology

In order to analyse morphological differences between derived titanosauriform clades, we digitized the appendicular skeleton of the holotypic and referred material of 21 somphospondylan species from the Gondwanan and European (Laurasian) Cretaceous record (Table 1). Most of these taxa are referable to Titanosauria, except for *Ligabuesaurus leanzai*, regarded here as an early member of Somphospondyli (following Mannion et al. 2019) and added as an outgroup in the comparisons. Each specimen also includes two different

Table 1 Sample of analysed somphospondylan sauropods

Taxon/Morphotype	OTU	Clade	Forelimb			Hindlimb		
			Humerus	Ulna	Radius	Femur	Tibia	Fibula
Aeolosaurus sp.	*Aeolosaurus*	Aeolosaurini	1	3	1	1	1	1
Antarctosaurus wichmannianus	*Antarctosaurus*	Titanosauria	1	–	–	1	1	1
Argentinosaurus huinculensis	*Argentinosaurus*	Colossosauria	–	–	–	–	–	1
Bonatitan reigi	*Bonatitan*	Lithostrotia	1	–	–	1	1	1
Bonitasaura salgadoi	*Bonitasaura*	Lithostrotia	–	–	–	1	2	1
Elaltitan lilloi	*Elaltitan*	Lithostrotia	1	1	1	1	1	1
Jainosaurus cf. *septentrionalis*	*Jainosaurus*	Titanosauria	1	–	–	1	1	1
Ligabuesaurus leanzai	*Ligabuesaurus*	Somphospondyli	1	–	–	1	1	1
Lirainosaurus astibiae	*Lirainosaurus*	Lithostrotia	3	–	–	3	1	3
Mendozasaurus neguyelap	*Mendozasaurus*	Colossosauria	1	1	1	1	1	1
Morphotype I at Lo Hueco	Morphotype I	Lithostrotia	4	6	3	10	10	9
Morphotype II at Lo Hueco	Morphotype II	Lithostrotia	7	4	1	9	5	8
Muyelensaurus pecheni	*Muyelensaurus*	Colossosauria	5	2	2	3	3	3
Narambuenatitan palomoi	*Narambuenatitan*	Lithostrotia	1	1	–	1	–	–
Neuquensaurus australis	*Neuquensaurus*	Saltasauridae	8	3	5	5	3	2
"*Neuquensaurus robustus*"	*Neuquensaurus*	Saltasauridae	1	2	–	3	2	1
Notocolossus gonzalezparejasi	*Notocolossus*	Colossosauria	1	–	–	–	–	–
Petrobrasaurus puestohernandezi	*Petrobrasaurus*	Titanosauria	1	–	–	2	1	–
Rinconsaurus caudamirus	*Rinconsaurus*	Colossosauria	1	–	–	–	–	–
Saltasaurus loricatus	*Saltasaurus*	Saltasauridae	5	4	4	4	4	2

Number of specimens for each element type

OTU operative taxonomic unit

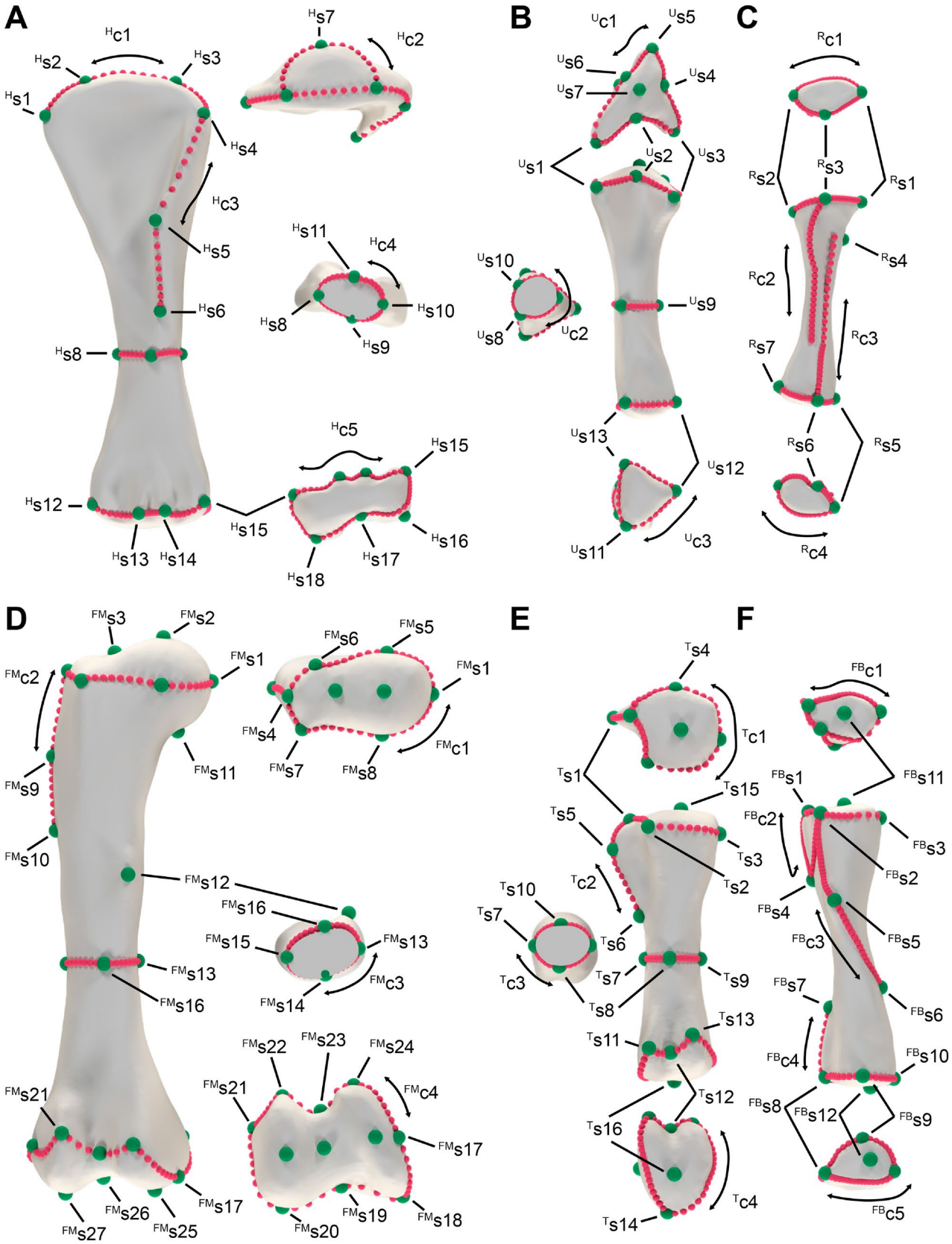
A
Hc1
Hs2
Hs3
Hs1
Hs4
Hc3
Hs5
Hs6
Hs8
Hs12
Hs13
Hs14
Hs7
Hc2
Hs11
Hc4
Hs8
Hs10
Hs9
Hc5
Hs15
Hs15
Hs16
Hs17
Hs18
B
Uc1
Us5
Us6
Us4
Us7
Us2
Us3
Us1
Us10
Us8
Uc2
Us9
Us13
Us12
Us11
Uc3
C
Rc1
Rs2
Rs3
Rs1
Rs4
Rc2
Rc3
Rs7
Rs6
Rs5
Rc4
D
FMs3
FMs2
FMc2
FMs1
FMs9
FMs11
FMs10
FMs6
FMs5
FMs1
FMs4
FMc1
FMs7
FMs8
FMs12
FMs16
FMs15
FMs13
FMs13
FMc3
FMs16
FMs14
FMs22
FMs23
FMs24
FMs21
FMc4
FMs17
FMs21
FMs17
FMs26
FMs27
FMs25
FMs19
FMs18
FMs20
E
Ts4
Tc1
Ts1
Ts15
Ts5
Ts3
Ts2
Ts10
Tc2
Ts7
Ts6
Tc3
Ts7
Ts9
Ts8
Ts13
Ts11
Ts12
Ts16
Tc4
Ts14
F
FBc1
FBs1
FBs11
FBc2
FBs3
FBs2
FBs4
FBc3
FBs5
FBs7
FBs6
FBc4
FBs10
FBs8
FBs12
FBs9
FBc5

◂**Fig. 2** Landmark and semilandmarks used in this study. Humerus in anterior, proximal, midshaft section and distal views (**a**), ulna in proximal, anterior, midshaft section and distal views (**b**), radius in proximal, posterior and distal views (**c**), femur in posterior, proximal, midshaft section and distal views (**d**), tibia in proximal, lateral, midshaft section and distal views (**e**) and fibula in proximal, lateral and distal views (**f**). Landmarks in green, semilandmark curves in red

grouping labels; one of them is a taxonomic label at genus level (e.g. *Neuquensaurus australis* and "*Neuquensaurus robustus*" are here included as *Neuquensaurus*, see Otero 2010, Salgado et al. 2005, the morphological variability does not support two different taxa and it is still debated whether they are different taxa or possible dimorphs). The other label is the more inclusive group (for the example above *Neuquensaurus* → Saltasauridae) to which they are inferred to belong in recent phylogenetic hypotheses proposed in the literature (Gorscak and O'Connor 2016; Poropat et al. 2016; Carballido et al. 2017; Díez Díaz et al. 2018a, b; Sallam et al. 2018; González Riga et al. 2018, 2019; Mannion et al. 2019). We have considered the in-group relationships of Colossosauria proposed by González Riga et al. (2019). However, the position of Colossosauria is still being debated, as some of its members or the entire group has been found to be deeply-branching members of Titanosauria outside Lithostrotia (e.g. Carballido et al. 2011, 2017) whereas most recent analyses position most of its members or recover the entire clade within Lithostrotia (e.g. Poropat et al. 2016, Díez Díaz et al. 2018a, b, Sallam et al. 2018, González Riga 2019; Gorscak O'Connor recovered most of its members within Lithostrotita except for *Argentinosaurus huinculensis*). We considered Colossosauria as early-branching members of Lithostrotia.

A 3D digital model representative of each specimen was obtained via stereophotogrammetry following the method of Mallison (2011; see also Mallison and Wings 2014). The specimens were photographed with a Canon EOS 1100D and Canon EOS 80D with Canon EFS 18–55 mm f3.5–5.6, Canon 50 mm f1.8 and Sigma 17–50 mm f2.8 lenses. The point cloud reconstructions were processed in Agisoft Photoscan™ v1.4.1. and the 3D mesh objects were exported in ".obj" format and post-processed with Blender v1.8 (Blender Online Community 2018). Some of the elements were digitized in an early stage of this research via an IR device with an Xbox 360 Kinect™ sensor (following the methods of Falkingham 2013). A comprehensive list of the sampled specimens and the digitizing method used for each can be accessed in the Online Resource 1. The sample of limb elements was analysed with the GMM tool-kit as it permits comparison of specimens of different sizes and sides of the skeleton, as well as the extraction of latent effects. For example, one common latent effect is a relationship between the size and shape of the skeletal elements which likely reflects ontogenetic variability due to development or other scaling processes (see Zelditch et al. 2012) which are beyond the scope of the current study. Our sets of landmark definitions are mostly type I and type II as per the classification of Bookstein (1991). Analysis of curved morphological features (e.g.. features like the deltopectoral crest of the humerus, cnemial crest of the tibia, lateral trochanter of the fibula) was possible with the use of curved semilandmarks (Gunz et al. 2005; Gunz and Mitteroecker 2013). We also analysed the complete surface of each specimen by using high density surface semilandmarks (see also Gunz et al. 2005) in a separate analysis of the complete morphology of each anatomical element (see below).

For the sliding of semilandmarks we followed the methodology originally proposed by Souter et al. (2010) modified by Botton-Divet et al. (2015). We created an "Atlas" or template mesh for each anatomical element in which the landmark and semilandmark curves are defined. Then, the curve semilandmarks are slid from the template to match the morphology of each analysed specimen (see Online Resource 2 for a step-by-step procedure). Landmark and semilandmark definitions, and placement of them in the template and the sampled specimens were made in the IDAV Landmark™ editor v3.0.7 (Wiley et al. 2005).

A list of the landmarks as well as curved and surface semilandmarks defined in each anatomical element can be accessed here (Fig. 2, Table 1). A comprehensive definition of each landmark and semilandmark used in this study can be accessed in Online Resource 2, with the percentage of missing information across the dataset. The landmarks were imported into R v.3.6.1. statistical software (The R Core Team 2016) in order to run a Generalized Procrustes Analysis (GPA) to align the landmark configurations of all the specimens and then explore morphospaces. The curve and surface semilandmarks were projected to the surface of each specimen via a Thin Plate Spline (TPS) algorithm which minimizes the Bending Energy (Gunz et al. 2005). Both procedures (sliding of the semilandmarks and GPA) were run with the *Morpho* v.2.7 (Schlager 2017) and *geomorph* v.3.1.2 (Adams et al. 2019) packages for R, respectively. The high density surface semilandmarks were generated as a retopologized quadratic mesh with the number of vertices equal to the number of desired semilandmarks using the software Instant Mesher v1.0 (Jakob et al. 2015). The retopologizing process generated a regular pattern of polygon faces with almost equal area across the entire mesh (Fig. 3d). The vertices of these faces were then transformed into semilandmark coordinates and slided over the template mesh using the *Morpho* and the *rgl* v.0.100.30 package for R (Adler et al. 2019; see Fig. 3d, e).

One of the most common problems in morphometric studies of paleontological material, especially those examining sauropod limb elements is the lack of completeness of all the morphological features in some of the available remains

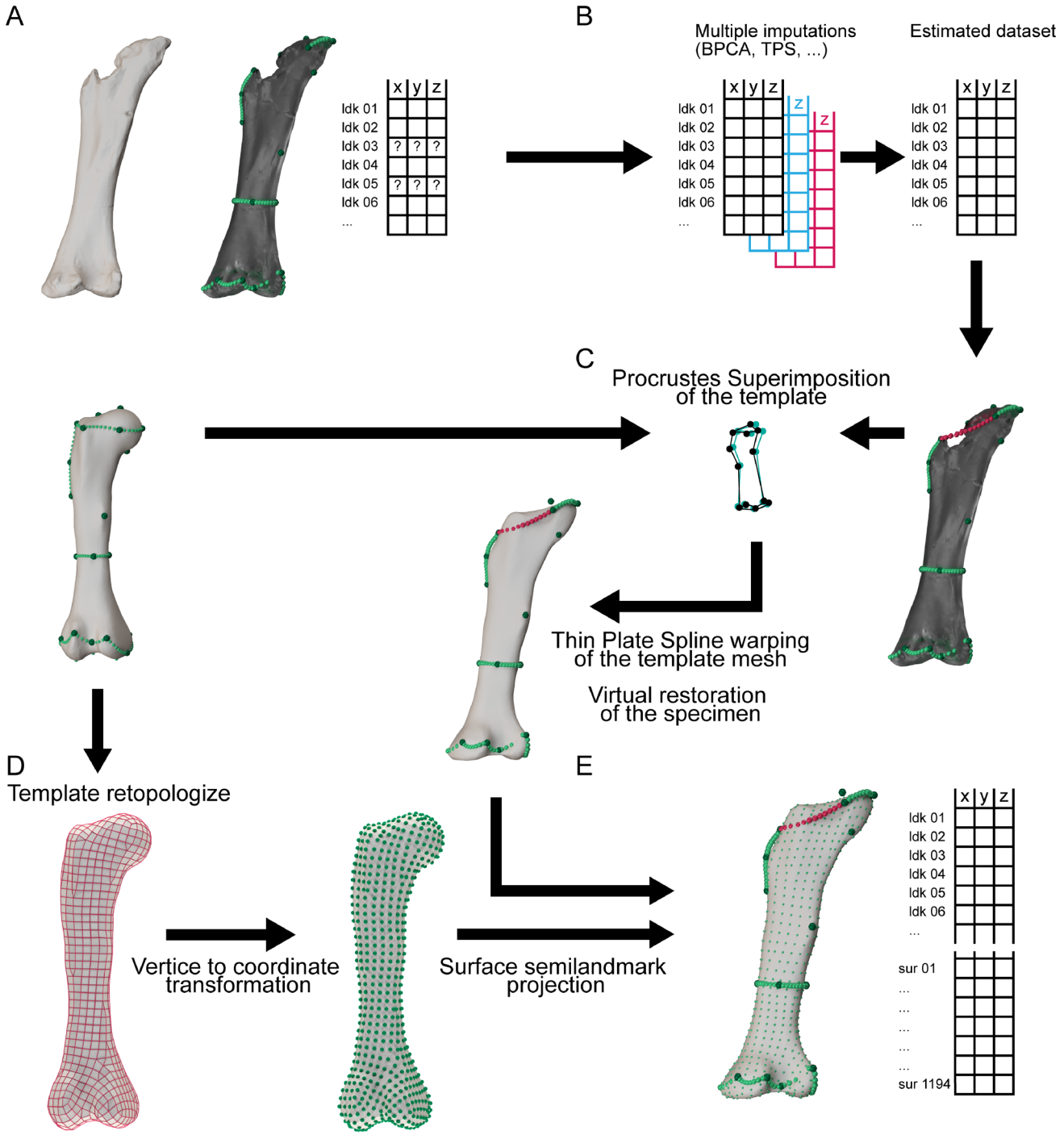

Fig. 3 Summary of landmark estimation and surface semilandmark projection procedure. Initial 3D mesh representation of the fossil specimen with an incomplete (not preserved) surface and landmark dataset (**a**), multiple imputation of the landmark dataset performed to produce the estimated set of x–y–z coordinates of the missing landmarks (**b**), superimposition of the template mesh and warping to the specimen's estimated landmark coordinates (**c**), retopologizing of the template mesh and conversion of these vertices into high-density surface semilandmarks (**d**) and projection of the high-density surface semilandmarks into the virtually restored specimen's mesh to generate the surface semilandmark dataset for the specimen (**e**)

(Lautenschlager 2017). It is common that many of the appendicular elements do not preserve part of the proximal and distal ends of the specimen (and this is particularly common in the Ibero-Armorican titanosaurians: e.g., Le Loeuff 2005; Vila et al. 2012; Díez Díaz et al. 2013; Ortega et al. 2015). A complete landmark and semilandmark configuration is

needed for the analyses, as well as the complete surface reconstruction of the specimen in order to process the sliding of the semilandmarks. However, manual manipulation of the 3D mesh (see virtual restorations by Lautenschlager et al. 2012; Molnar et al. 2012; Vidal and Díez Díaz 2017) can introduce biases due to subjective morphological assumptions that are not desirable in the analysis of the morphology. Therefore, we instead relied on virtual statistical restoration methods and elected to use the techniques provided by the GMM tool-kit (Gunz et al. 2009; Profico et al. 2018; Schlager et al. 2018). We used multiple imputation methods to estimate the missing landmarks for use in TPS analyses following the procedure of Gunz et al. (2009) in *geomorph* (see Fig. 3a, b). After a complete set of landmarks and semilandmarks was obtained, the specimen complete surface mesh was generated also using the TPS algorithm to warp the template mesh to the new configuration (following Gunz 2005; see also Botton-Divet et al. 2015; Fig. 3c). These reconstructed meshes were used to project the high-density surface semilandmarks on each specimen and create the surface dataset. After being projected for each specimen, the surface semilandmarks were positioned by sliding prior to performing the GPA (Table 2).

After positioning the landmarks and the GPA, the resulting Procrustes coordinates (translated into shape space) were used in two different ways. The landmark and curve semilandmark dataset with the main morphological features of the element was analysed via Principal Component Analysis (PCA; e.g. Strauss and Bookstein 1982; Zelditch et al. 2012) in order to characterize large-scale aspects of the morphological variation. They were also analysed with Linear Discriminant Analysis (LDA; see Darlington et al. 1973) to observe group differences between the a priori classifications (in this case, more exclusive group relationships within somphospondylan sauropods, such as Titanosauria, Lithostrotia and Saltasauridae). LDA finds linear combinations of variables that describe intergroup variance (the Linear Discriminant—or LD; see Claude 2008; Mitteroecker and Bookstein 2011) using a scaling function based on Mahalanobis distances (Darlington et al. 1973; Claude 2008) while taking into account the within-group variance–covariance matrix. This allow us to: (1) analyse morphospace occupation while maximizing the morphological differences between the derived titanosaurian specimens included in the current dataset and the other specimens studied; (2) discuss paleobiological implications of the differences between the morphological LDA results and the morphological PCA results. The PCA on the Procrustes coordinates was performed to evaluate morphological variation within the sample without emphasizing a priori group differences in the calculation with the basic *prcomp*() function. LDA was performed with the *MASS* v.7.3–51.4 package (Venables and Ripley 2002). Herein we present the main Principal Components (PCs) and LDs results, with emphasis on those capturing the main morphological variation (e.g. PC1 and PC2, LD1 and LD2). The PCAs on the forelimb elements can be found with a mesh representation of the morphology plotted at each extreme of the PC (Fig. 4), and similarly with the PCAs of the hindlimb elements (Fig. 5). The comprehensive report on the complete PCA and LDA results can be accessed in Online Resource 3. We also tested the statistical differences between the different titanosaurian clades via Kruskal Wallis and Mann–Whitney U pairwise comparison with a post-hoc Bonferroni p value adjustment. These tests were carried out to assess if there were significant differences between the different exclusive groups in the shape PCAs. Results of the Kruskal Wallis test can be accessed in Table 3, and Mann–Whitney U pairwise comparison in Table 4. Also, a supplementary test between the different taxonomic units used in this study is provided in Online Resource 3.

The high-density semilandmarks are used to analyse the morphological features exhibiting most of the variation between the different clades. Instead of exploring the morphospace occupation, LDA was applied on the high-density surface semilandmarks to calculate the morphological variation maximizing the between group differences in a phylogenetic context by assigning specimens to groups according to their "clade" label. The resulting LDs were then used to calculate the morphological differences between the extreme configurations. The LDA "eigenvectors" (in LDA the eigenvector is a scaled decomposition using the within group variance; see also Claude 2008) were obtained and used to calculate the extreme surface semilandmark configurations for each LD. Then, the Procrustes distances (see Rohlf 2000) were calculated between the surface semilandmark configurations for the extreme values of each Linear Discriminant. Procrustes distances were approximated with Euclidean distances between the surface semilandmark coordinates assuming that there is low variation between them (Kendall 1984; Rohlf 1998 1999). After this calculation, we obtained the Procrustes distances for each of the high-density surface semilandmarks, which allowed to visualize the areas of maximum variation in morphology for each element. This also allowed us to compare where most of the between-group variance is concentrated against previous osteological characters as described in current sauropod systematic analyses (e.g. Carballido et al. 2017; González Riga et al. 2019) or if it is found to correspond weakly, could potentially be used to define new osteological characters in future studies.

Table 2 Landmark and semilandmark definitions for the current study

	N of Landmarks	Landmarks	N	Semilandmarks Curves determination		Missing (%)
Humerus	18	s1–s18				11.99
			30	c1		29.54
			20	c2		34.09
			20	c3		20.45
			40	c4		6.82
			70	c5		38.63
			1651		Surface	–
Ulna	12	s1–s6, s8–s13				12.65
			60	c1		33.33
			30	c2		0.00
			30	c3		29.63
			1651		Surface	–
Radius	7	s1–s7				2.78
			46	c1		11.11
			28	c2		5.56
			28	c3		0.00
			41	c4		11.11
			1628		Surface	–
Femur	24	s1–s24				16.83
			50	c1		44.00
			20	c2		14.00
			40	c3		6.00
			60	c4		40.00
			1624		Surface	–
Tibia	14	s1–s14				14.66
			41	c1		28.95
			19	c2		26.32
			40	c3		0.00
			50	c4		47.37
			1412		Surface	–
Fibula	10	s1–s10				11.35
			40	c1		24.32
			40	c2		21.62
			44	c3		8.11
			10	c4		24.32
			40	c5		29.73
			719		Surface	–

3 Results

3.1 Morphospace occupation within titanosauria

3.1.1 Humerus

The PCA of the humeri recovered 44 PCs, with the first seven PCs summarizing 81.99% of the cumulative variance. The LDA recovered five LDs, with the first two LDs summarizing 80.71% of the cumulative variance. The PCA results highlight differences between the robust humeri of saltasaurids (e.g. *Saltasaurus loricatus*) and the slender and more anteriorly projected humeri in members of Rinconsauria (e.g. *Muyelensaurus pecheni*, MRS-Pv-70), which exhibits positive values in PC1 (Fig. 4). PC1 (which accounts for 45.84% of the variance) plots more robust humeri with especially mediolaterally expanded proximal ends at negative values whereas more gracile humeri with slightly anteriorly-placed deltopectoral crests plot at more positive values (Fig. 4a, b). PC2 (11.93% of the variance) captures differences in the rotation of the deltopectoral crest, the expansion of the proximal and distal ends, and

the curvature of the shaft (displacement of the proximal end relative to the midshaft width and the distal end in mediolateral and lateral views). The straighter and slightly more robust elements lacking strong anterior projection of the deltopectoral crest plot at more negative values (Fig. 4a, b). Specimens with greater shaft curvature and more anteriorly projected deltopectoral crest plot in more positive values (Fig. 4a, b). There are slight differences among non-lithostrotian members referred to Titanosauria (e.g. *Antarctosaurus wichmannianus* specimen MCNA-6804), colossosaurs and some saltasaurids, which plot at more negative values of PC2, whereas most lithostrotian titanosaurs are plotted near zero or exhibit slightly negative values (Fig. 4a). However, overlapping between non-lithostrotian and lithostrotian sauropods is common along PC2. Specimens of *Muyelensaurus pecheni* and *Saltasaurus loricatus* occupy the largest ranges in PC2. In the case of *Muyelensaurus* specimens range from near zero value of PC2 in some specimens which exhibit a slightly medially-rotated deltopectoral crest (e.g. MAU-PV-357) whereas some specimens plotting with more positive values have an unrotated, anteriorly projected deltopectoral crest (e.g. MAU-PV-70). LDA results also allow the identification of large differences between the members of Saltasauridae and other somphospondylans, as well as major differences between non-titanosaur somphospondylans and other titanosaurs. LD1 (which account for 62.91% of the variance) plots saltasaurids at positive values, far from the values occupied by other titanosaurian sauropods. The other non-saltasaurid titanosaurs are plotted at negative values of LD1 (Fig. 5b). The members of Colossosauria plot at more negative values of LD1 slightly separated from other titanosaurians and slightly separated from other lithostrotians, and only slightly overlapping with the humeri referred to Morphotype II at Lo Hueco (Fig. 6a). LD2 (which accounts for 19.01% of the variance) highlights major differences between the non-titanosaurian somphospondylan *Ligabuesaurus leanzai*, which plots isolated at more negative values of LD2, and the other titanosaurs. Non-lithostrotian titanosaurs plot at modestly negative values overlapping with non-colossosaurian and non-saltasaurid lithostrotians (Fig. 4a), whereas Colossosauria generally plot near zero with slightly negative values of LD2, slightly overlapping with Morphotype II at Lo Hueco (Figs. 4a, b, 6a). Except for some specimens from Morphotype II at Lo Hueco (i.e. HUE-1647, HUE-3829), most non-saltasaurid lithostrotians plot at negative values of LD2.

The LDA results resemble the subclade separations of the PCA (Figs. 4a, 6b) despite some major differences in the position of *Ligabuesaurus leanzai* in the morphospace and the extent of morphological differences between the non-lithostrotian titanosaurs and members of Lithostrotia (Fig. 6). Members of Colossosauria plot separated from other somphospondylan sauropods in both analyses. However, some differences can only be observed when the clade differences are maximized in the LDA. The more deeply-nested colossosaurian sauropods (e.g. *Mendozasaurus neguyelap* and *Notocolossus gonzalezparejasi*; Fig. 5a) share an area of the morphospace occupation with both other non-lithostrotian and lithostrotian sauropods, whereas Rinconsauria is separated off on its own in the PCA. In contrast, the LDA plots essentially a slightly separated Colossosauria in their own region of the morphospace with the more early branching colossosaurs (e.g. *Rinconsaurus caudamirus*) closer to the region of the morphospace occupied by other non-lithostrotian titanosaursand non-colossosaurian lithostrotians (Fig. 6a). Morphotype II at Lo Hueco and *Lirainosaurus astibiae* are the lithostrotian titanosaurs that plotted nearest the region of the morphospace occupied by rinconsaurian colossosaurs (Fig. 6a).

3.1.2 Ulna

The PCA of the ulnae recovered 27 PCs, of which the first five PCs summarize 83.93% of the variance. In contrast, the LDA of the ulnae recovered only three LDs with the first LD summarizing 81.61% of the variance. PC1 (which accounts for 57.19% of the variance) highlights differences between the extremely slender ulnae of Morphotype II at Lo Hueco and *Mendozasaurus neguyelap*, which both plot at more negative values, and the robust ulnae of saltasaurids which plot at more positive values of PC1 (Fig. 4). In this analysis, the saltasaurids overlap slightly with other lithostrotian titanosaurs, in part because specimens of *Neuquensaurus* spp. exhibits few differences from those of *Aeolosaurus* sp. and Morphotype I at Lo Hueco (among others; see Fig. 4c–e).

PC2 (which accounts for 10.0% of the variance) summarizes morphological differences between the mediolateral expansion and the relative shape of the olecranon process. Such variation is evenly distributed among all the sampled titanosaurian clades. No noteworthy differences were found among the values of the different titanosaurian clades across this PC.

LD1 (which accounts for 81.61% of the variance) separates deeply-nested titanosaurs, specifically members of the Saltasauridae and *Aeolosaurus* sp, (e.g. specimen MPCA-Pv-27174) at negative values from all the other titanosaurians (including early branching lithostrotians) which plot at positive values of LD1 (Fig. 6b). LD2 (which account for 12.32% of the variance) does not significantly separate the titanosaurian specimens, all of which plot at negative values or near zero (Fig. 5d). Some titanosaurian specimens plot at slightly positive values whereas colossosaurian ulnae plot at positive values of LD2, separated from the region of other titanosaurs in the morphospace. The overlapping between saltasaurids and *Aeolosaurus* spp. Is noteworth, since they exhibit short, robust ulnae with anteroposteriorly-wide

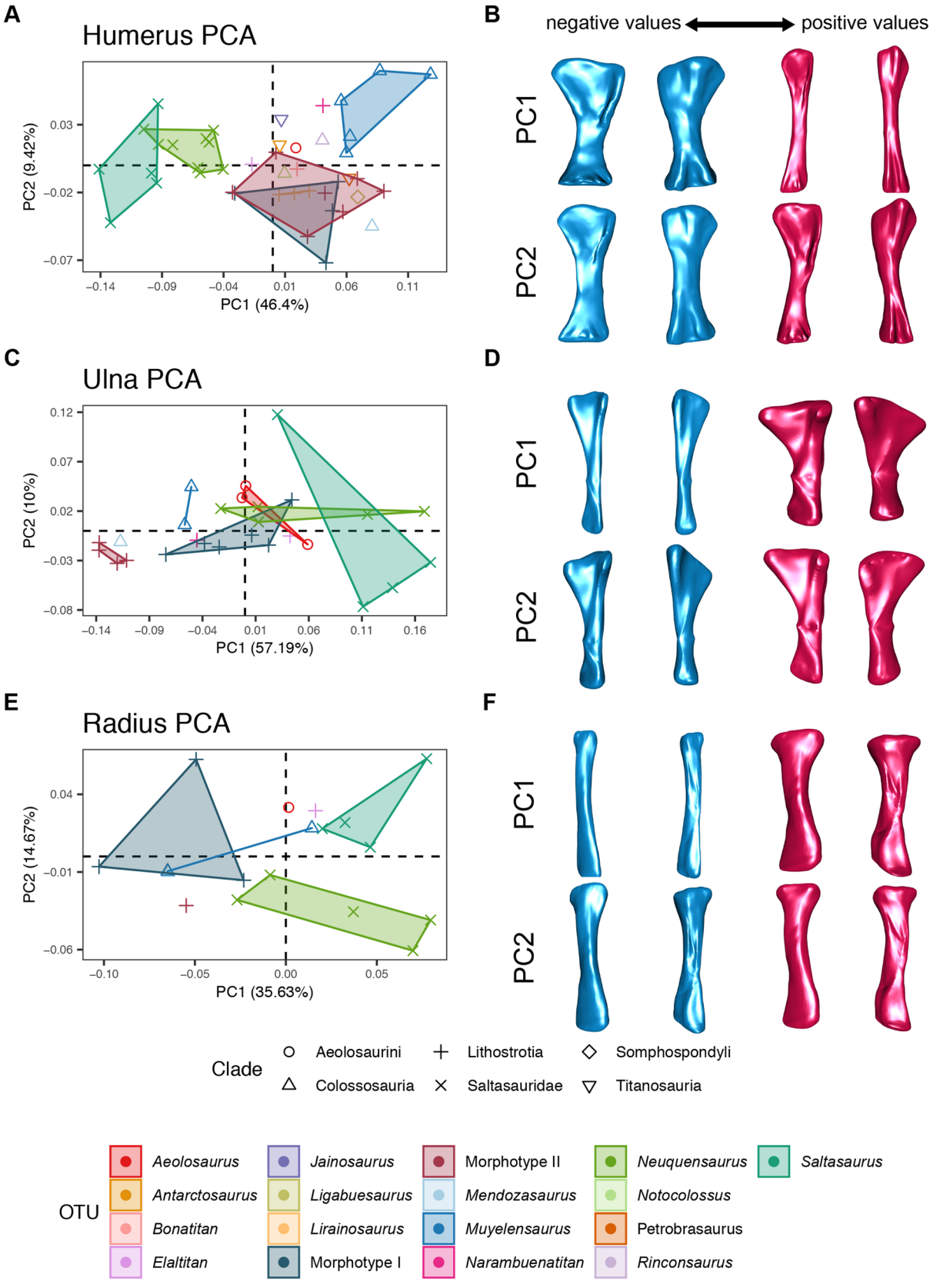
A
Humerus PCA
PC2 (9.42%)
PC1 (46.4%)
B
negative values
positive values
PC1
PC2
C
Ulna PCA
PC2 (10%)
PC1 (57.19%)
D
PC1
PC2
E
Radius PCA
PC2 (14.67%)
PC1 (35.63%)
F
PC1
PC2
Clade
Aeolosaurini
Lithostrotia
Somphospondyli
Colossosauria
Saltasauridae
Titanosauria
OTU
Aeolosaurus
Antarctosaurus
Bonatitan
Elaltitan
Jainosaurus
Ligabuesaurus
Lirainosaurus
Morphotype I
Morphotype II
Mendozasaurus
Muyelensaurus
Narambuenatitan
Neuquensaurus
Notocolossus
Petrobrasaurus
Rinconsaurus
Saltasaurus

◂**Fig. 4** PCA results over the GPA aligned landmark and semilandmark curves of the forelimb skeletal elements. PCA of the sample of humeri (**a**), representation of humeral shape change along PC1 and PC2 respectively (**b**), PCA of the sample of ulnae (**c**), representation of the ulnar shape change along PC1 and PC2 respectively (**d**), PCA of the sample of radii (**e**) and representation of the radial shape change along PC1 and PC2 respectively (**f**). Mesh representation portray negative values in blue, positive values in red. *OTU* operative taxonomic unit/morphotype. Shape and colour legend indicated in the bottom of the image

anteromedial processes and bulbous and mediolaterally-wide olecranon processes, as no other analysis show overlapping between these two forms, especially in the LDA analyses.

3.1.3 Radius

The PCA of the radii recovered 18 PCs, with the first six summarizing 81.64% of the total variance. The LDA resulted in three LDs with the first two summarizing 92.21% of total variance. PC1 (which accounts for 35.63% of the variance) highlights the robustness difference between the straight and slender radius of *Muyelensaurus pecheni* and both morphotypes from Lo Hueco, which plot at more positive values (Fig. 4e, f). Certain specimens of *Neuquensaurus* spp. (e.g. MLP-CS-1167), *Aeolosaurus* sp. (specimen MPCA-Pv-27174) and *Elaltitan lilloi* plot near zero, whereas the robust and slightly curved radii of *Saltasaurus loricatus* and many of the *Neuquensaurus* spp. specimens plot at negative values of PC1. PC2 (which accounts for 14.67% of the variance) highlights differences between straighter radii with more acute posterior ridges and slightly more anteroposteriorly compressed shaft plot at negative values (Fig. 4e, f). Specimens plotting at positive values exhibit more anteroposteriorly expanded and rounded proximal and distal ends, with a more markedly projected ridge ascending from the posteromedial corner of the distal condyle (pmdc following Upchurch et al. 2015).

In contrast, the LDA found considerable differences among all the titanosaurian subclades. LD1 (which accounts for 52.1% of the variance) presents members of Colossosauria at more negative values while *Aeolosaurus* sp. and Morphotype I plot at less negative values. Many lithostrotian specimens overlap near zero values on this axis. A single radius from Morphotype I and *Elaltitan lilloi* overlap with Saltasauridae at less positive values (Fig. 5d). LD2 (which accounts for 40,12% of the variance) identifies differences between non-colossosaurian and non-saltasaurid titanosaurs (Morphotype I and Morphotype II at Lo Hueco and *E. lilloi*) which plot at negative values, whereas Colossosauria and Saltasauridae exhibit slightly negative to positive values. (Fig. 6c). There is a large overlap between the specimens of colossosaurs, saltasaurids and *Aeolosaurus* sp. at positive values on this axis, indicating minimal morphologic differences among the radii of these three distinct titanosaurian subclades.

3.1.4 Femur

The PCA of the analysed femora resulted in 50 PCs with the first eight PCs summarizing 81.52% of the total variance. The LDA on the other hand resulted in five LDs with the first three LDs summarizing 86.89% of the total variance. PC1 (which accounts for 32.72% of the variance) highlights the overlapping of most of the members of non-saltasaurid and non-aeolosaurini Somphospondyli across this axis (Fig. 5a, b). the members of Saltasauridae, *Aeolosaurus* sp. (specimen MPCA-Pv-27177), *Bonitasaura salgadoi*, *Narambuenatitan palomoi* and *Elaltitan lilloi* plot at more positive values, and these specimens exhibit a robust femora with anteroposteriorly expanded proximal and distal ends, a less eccentric shaft and the distal condyles slightly rotated towards medial (Fig. 5a, b). Along PC2 (which accounts for 17.3% of the variance) the specimens with the shaft medially deflected, slightly quadrangular proximolateral corner of the proximal end in anterior view and proximally positioned minimum midshaft width plot at negative values. As values along PC2 becomes more positive, the specimens exhibit progressively more columnar femora, with a slight expansion of the proximal and distal ends and more distally-placed minimum midshaft width (Fig. 5a, b). All the sampled somphospondylans overlap in values along this PC indicating variable morphologies that are similar between the sampled specimens of different subclades (Fig. 5a).

The LDA resulted in a separation of most of the sauropod group morphospaces despite the low sample size in some of the studied subclades (e.g. non-lithostrotian titanosaurians, Fig. 6d). LD1 (which account for 45.25% of the variance) plots *Ligabuesaurus leanzai*, non-saltasaurid lithostrotians and *Aeolosaurus* sp. at more negative values (Fig. 6d). The members of Colossosauria are plotted near zero towards more negative values, overlapping in some values with other non-saltasaurid lithostrotians (Fig. 6d), whereas the members of Saltasauridae are plotted separated from other somphospondylans at positive values of LD1 (Fig. 6d). LD2 (which accounts for 26.33% of the variance) highlights the differences between *L. leanzai* and lithostrotian titanosaurs which plot at negative values, whereas specimens of non-lithostrotian titanosaurs are plotted exclusively at positive values of LD2. The non-lithostrotian titanosaurs and Colossosauria overlap at similar values in the PCA whereas the LDA allows the non-lithostrotian titanosaurs and Colossosauria to be separated along LD1.

Elaltitan lilloi, *Narambuenatitan palomoi* and *Aeolosaurus* sp. possess femora that resemble those of saltasaurids (see PCA, Fig. 5a), but only *E. lilloi* was recovered at a position slightly closer to the saltasaurids in the LDA (yet

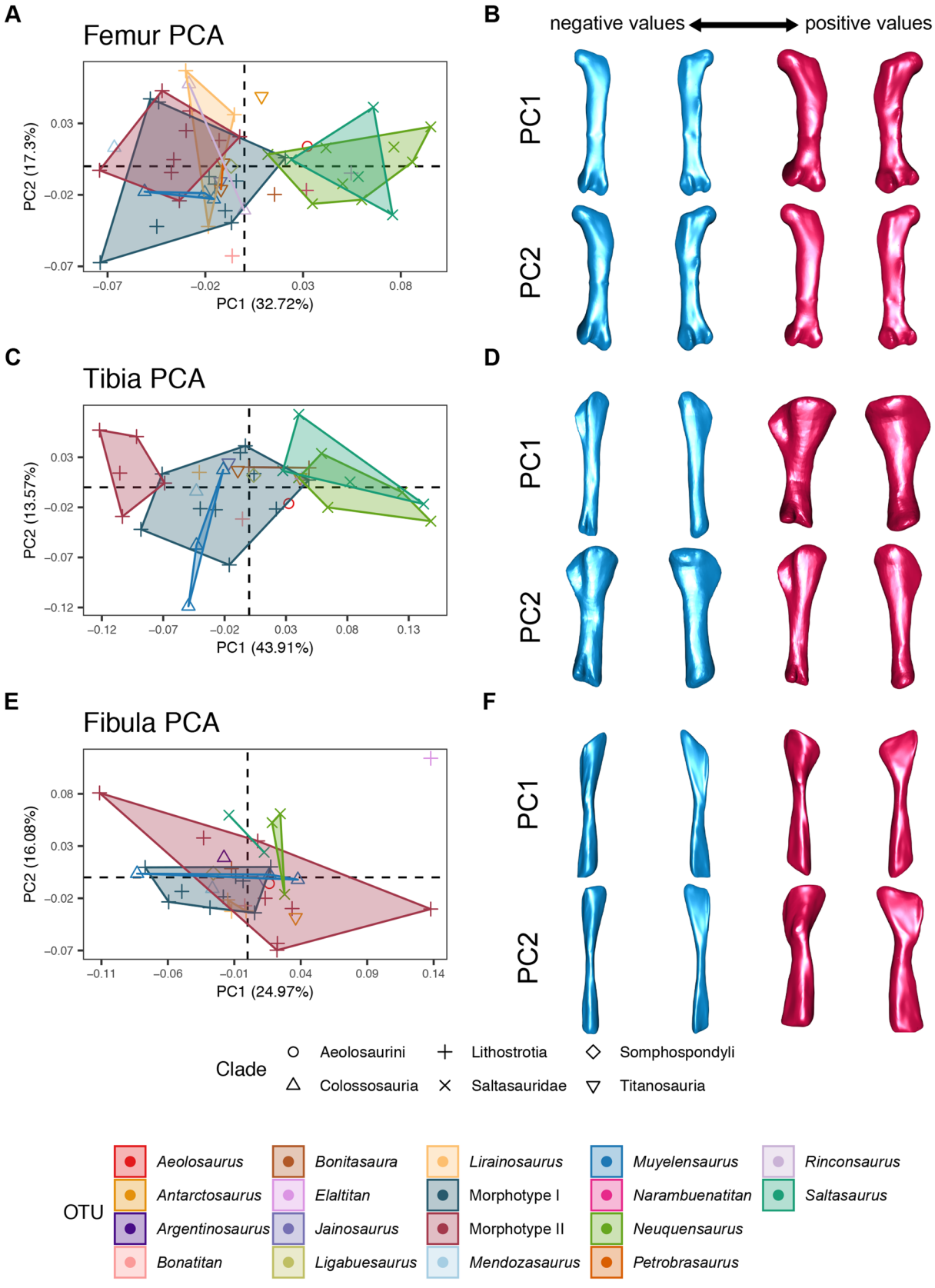
A
Femur PCA
PC2 (17.3%)
PC1 (32.72%)
B
negative values
positive values
PC1
PC2
C
Tibia PCA
PC2 (13.57%)
PC1 (43.91%)
D
PC1
PC2
E
Fibula PCA
PC2 (16.08%)
PC1 (24.97%)
F
PC1
PC2
Clade
Aeolosaurini
Lithostrotia
Somphospondyli
Colossosauria
Saltasauridae
Titanosauria
OTU
Aeolosaurus
Antarctosaurus
Argentinosaurus
Bonatitan
Bonitasaura
Elaltitan
Jainosaurus
Ligabuesaurus
Lirainosaurus
Morphotype I
Morphotype II
Mendozasaurus
Muyelensaurus
Narambuenatitan
Neuquensaurus
Petrobrasaurus
Rinconsaurus
Saltasaurus

◂**Fig. 5** PCA results over the GPA aligned landmark and semilandmark curves of the hindlimb skeletal elements PCA of the sample of femora (**a**), representation of femoral shape changes along PC1 and PC2 respectively (**b**), PCA of the sample of tibiae (**c**), representation of tibial shape changes along PC1 and PC2 respectively (**a**), PCA of the sample of fibulae (**e**) and representation of fibular shape changes along PC1 and PC2 respectively (**f**). Mesh representation portray negative values in blue, positive values in red. *OTU* operative taxonomic unit/morphotype. Shape and color legend indicated in the bottom of the image

still far from their morphospace; see Figs. 5, 6). *Narambuenatitan palomoi* and *Aeolosaurus* sp. (specimen MPCA-Pv-27177) exhibit femoral morphologies similar to those of non-saltasaurid lithostrotian.

3.1.5 Tibia

The PCA of the tibiae recovered 38 PCs with the first six PCs summarizing 81.77% of variance. The LDA recovered only five LDs with the first three LDs summarizing 87.87% of the total variance. PC1 (which accounts for 57.87% of the variance) places the extremely gracile and elongated tibiae of the specimens of Morphotype II at Lo Hueco at highly negative values (Fig. 5c). At less negative values the tibiae progressively exhibit a more anteroposteriorly-expanded proximal end and mediolaterally-expanded distal end (Fig. 5). The robust and mediolaterally expanded tibiae of the saltasaurids plot at positive values of PC1 (Fig. 5c, d). PC2 (which accounts for 13.57% of the variance) recovered the tibiae with a more anteroposteriorly-expanded proximal end and more mediolaterally-expanded distal end, and the anteriorly-projected articular surface of the ascending process plotted at more negative values (Fig. 5c, d). In contrast, positive values highlights specimens with tibiae with the proximal end is expanded anteroposteriorly as it is mediolaterally, a slightly more compressed distal end and less developed articular surface for the ascending process.

The LDA found considerable differences between the saltasaurids, *Ligabuesaurus leanzai*, most non-saltasaurid lithostrotians and non-colossosaurian titanosaurians, Titanosauria and Colossosauria (Fig. 6e). LD1 (which accounts for 63.25% of the variance) highlights differences between the specimens of Saltasauridae and *L. leanzai* which plot at negative values, with *Neuquensaurus* specimens slightly overlapping with the tibiae of *Bonatitan reigi* and specimens ofMorphotype I of Lo Hueco. These taxa are also recovered in LD1 near the specimens of *Aeolosaurus* sp. (specimen MPCA-Pv-27100-8), *Jainosaurus* cf. *septentrionalis* and *Bonitasaura salgadoi* which plot at lower negative values and zero in this axis (Fig. 7d). Some of the specimens of non-lithostrotian titanosaurs (e.g. *J.* cf. *septentrionalis*) and *Aeolosaurus* sp. are plotted at slightly negative values and zero (Fig. 6e), but the majority of the members from Lithostrotia plot between zero and positive values of LD1 (Fig. 6e). Members of Colossosauria plot at increasingly positive values, with the specimens of *Mendozasaurus neguyelap* closer to the values in which the specimens of other non-colossosaur lithostrotian are plotted (Fig. 6e). LD2 (which accounts for 20.14% of the variance) differentiates the saltasaurid, *Aeolosaurus* sp. and colossosaurian titanosaurs from the other somphospondylan subclades. Specimen MPCA-Pv-27100-8 of *Aeolosaurus* sp.plots at negative values, near colossosaurs and saltasaurids which exhibit slightly less negative values on this axis (Fig. 6). Most other titanosaurian specimens are plotted between zero and positive values. The non-titanosaurian somphospondylan *L. leanzai* is plotted isolated at highly positive values of LD1 and negative values of LD2 (Fig. 6e).

3.1.6 Fibula

The PCA recovered 37 PCs, with the first seven PCs summarizing 81.81% of the total variance. The LDA recovered five LDs where the first three summarize 85.59% of the total variance. PC1 (which accounts for 24.97% of the variance) highlights the straight fibulae with more mediolaterally compressed shaft and medial deflection of the anterior trochanter, which are plotted at negative values (Fig. 6e, f). As PC1 values become positive, the fibulae exhibit more mediolateral expansion with a slightly more sigmoidal shaft and proximodistally-shorter anterior trochanter (Fig. 5e, f). PC2 (which accounts for 16.08% of the variance) plotted the slender fibulae with mediolaterally compressed and straight shaft at negative values (Fig. 5e, f). When PC2 values become more positive, the fibulae exhibit a more sigmoidal profile in lateral view and mediolaterally wider shaft and a more recurved lateral trochanter (Fig. 5e, f). According to this plot, most of the examined titanosaurian fibulae share a similar morphology, *Elaltitan lilloi* is the only taxon that exhibits a distinct morphology as evidenced by its plotting apart from other somphospondylan specimens (Fig. 5e).

In contrast, the LDA was able to differentiate most of the titanosaurian subclades (Fig. 7f). LD1 (which accounts for 48.48% of the variance) plots non-colossosaurian lithostrotians and *Ligabuesaurus leanzai* at negative values, whereas the Colossosauria is plotted at the most positive values compared with all the other taxa considered (Fig. 6f). The non-lithostrotian titanosaurs are plotted at positive values of LD1, near the values of colossosaurian but at slightly lower values (Fig. 6f). The specimens of *Aeolosaurus* sp. and Saltasauridae are plotted near zero thus exhibiting few differences from other member of Somphospondyli which are also plotted at negative values of LD1 (Fig. 6f). LD2 (which accounts for 23.07% of the variance) plots early branching somphospondylans (non-saltasaurid and non-aeolosaurini somphospondylans) at negative values (Fig. 6f). Specimens

Table 3 Total results of the PCA and LDA over the procrustes coordinates in each element type

	PCs	PCs(> 80% variance)	N of PCs after Anderson's χ test	LDs	LDs (> 80% variance)
Humerus	44	PC1-PC6	43	5	LD1-LD2
Ulna	27	PC1-PC4	26	3	LD1
Radius	18	PC1-PC5	17	3	LD1
Femur	50	PC1-PC7	49	5	LD1-LD2
Tibia	38	PC1-PC5	37	5	LD1-LD2
Fibula	37	PC1-PC6	36	5	LD1-LD2

Table 4 Kruskal Wallis over the shape PCs; χ^2 and p values after Bonferroni correction

	Humerus		Ulna		Radius		Femur		Tibia		Fibula	
	Chi-sq	p value	Chi-sq	p value	Chi-sq	p value	Chi-sq	p value	Chi-sq	p value	Chi-sq	p value
PC1	31.568	0.000*	12.980	0.019*	9.184	0.108	27.626	0.000*	19.029	0.030*	4.984	1.000
PC2	14.685	0.071	4.733	0.770	2.260	1.000	1.122	1.000	3.623	1.000	7.702	1.000
PC3	2.272	1.000	0.035	1.000	2.307	1.000	11.328	0.271	6.859	1.000	10.888	0.858
PC4	3.560	1.000	3.213	1.000	5.582	0.535	6.391	1.000	10.641	0.944	9.143	1.000
PC5	3.862	1.000	3.876	1.000	6.193	0.410	4.381	1.000	1.980	1.000	5.731	1.000
PC6	2.942	1.000	1.019	1.000	1.783	1.000	4.460	1.000	4.854	1.000	19.237	0.028*
PC7	6.091	1.000	3.444	1.000	2.120	1.000	2.797	1.000	2.720	1.000	6.941	1.000
PC8	4.268	1.000	3.314	1.000	1.327	1.000	5.672	1.000	3.871	1.000	6.986	1.000
PC9	7.039	1.000	2.540	1.000	1.348	1.000	11.561	0.248	3.683	1.000	7.391	1.000
PC10	5.387	1.000	7.732	0.208	2.438	1.000	1.651	1.000	3.322	1.000	8.615	1.000

α = 0.05, significant p values indicated with '*'

of Saltasauridae and *Aeolosaurus* sp. (MPCA-Pv-27100-7) are plotted at positive values of LD2 (Fig. 6f).

Whereas most of the sauropods show similarities in the fibular morphology, members of Colossosauria and other non-lithostrotian titanosaurs exhibit major morphological differences in comparison with other analysed somphospondylans (Fig. 6f). In particular among colossosaurs, the fibulae of members of Rincosauria were found to differ the most when compared with other titanosaurs, which is evident graphically by the plotting of these specimens the farthest from other non-colossosaurian titanosaurian specimens along LD1. The specimens of *Muyelensaurus pecheni* are plotted at the most positive values of LD1, slightly overlapping with values of *Argentinosaurus huinculensis* but far from the other early-branching colossosaur *Mendozasaurus neguyelap* or the non-lithostrotian titanosaur specimens. In contrast, *M. pecheni* plots at negative values of LD2 separated from other members of Colossosauria and overlapping with the values in which other non-saltasaurid and non-aeolosaurini titanosaurs are plotted (Fig. 6f). In comparison, the PCA recovered no morphological divergence among the specimens of Colossosauria. Similarly, the lithostrotian titanosaurs (including *Elaltitan lilloi*) present a high variability at random among the different subclades as evidenced graphically by the PCA (Figs. 5e, 6f). Despite the slight morphological differences between the specimens of some taxa and the high variability recovered in the PCA, the LDA plot all the specimens of non-saltasaurid lithostrotian plotted in the same area of morphospace (positive values of LD1, zero to negative values of LD2). They do not differ greatly, unlike the PCA where *Ligabuesaurus leanzai* is plotted closer to Colossosauria and the *E. lilloi* specimen separate from the other titanosaurs examined (Fig. 7e, f).

3.2 Titanosaurian morphological differences

The Kruskal Wallis test on the results of the shape PCAs (Table 4) recovered only significant differences among the analysed clades in the PC1 of the humerii ($\chi^2 = 31.568$, $p < 0.05$), PC1 of the ulnae ($\chi^2 = 12.980$, $p < 0.05$), PC1 of the femora ($\chi^2 = 27.626$, $p < 0.05$), PC1 of the tibiae ($\chi^2 = 19.029$, $p < 0.05$) and PC6 of the fibulae ($\chi^2 = 19.237$, $p < 0.05$). The Mann–Whitney U pairwise test (Online Resource 3) recovered significative differences ($p < 0.05$ from now on) in PC1 of the humerii among colossosaurians, lithostrotians and saltasaurids, as well as between members of Saltasauridae and between members of Titanosauria separately. The test of PC1 of both the ulnae and the radii found significative differences between Saltasauridae and non-saltasaurid Lithostrotia, as well as between members

of Saltasauridae and Colossosauria. The test of PC1 of the femora found only significant differences in the comparison between members of Saltasauridae and Colossosauria, members of Saltasauridae and non-saltasaurid Lithostrotia and members of Saltasauridae and non-lithostrotian Titanosauria. The test of PC1 of the tibiae found significant differences in the comparison between members of Colossosauria and Saltasauridae and members of Lithostrotia and Saltasauridae. In contrast, the test of the fibula shape PCA found the least differences along its PCs, with no significant differences in the PC1. There are significant differences but only after PC1-PC2 (Fig. 5e), where our test found significant differences in PC6 between members of non-saltasaurid Lithostrotia and Saltasauridae (Online Resources 3–4).

A Kruskal Wallis test was also carried out on the LDA results (Table 5). It recovered significant differences among the analysed somphospondylans subclades in LD1 for all the element types. The test also found significant differences in LD2 of the humeri ($\chi^2 = 27.414$, $p < 0.05$), LD4 of the humeri ($\chi^2 = 20.976$, $p < 0.05$), LD5 of the humeri ($\chi^2 = 17.596$, $p < 0.05$). LD2 of the radii ($\chi^2 = 10.887$, $p < 0.05$), LD2 of the femora ($\chi^2 = 26.182$, $p < 0.05$), LD4 of the femora ($\chi^2 = 20.670$, $p < 0.05$), LD2 of the tibiae ($\chi^2 = 27.081$, $p < 0.05$) and LD2 of the fibulae ($\chi^2 = 18.839$, $p < 0.05$). The pairwise Mann–Whitney U's test (Online Resource 3) of the humeri found significant differences among Lithostrotia, Saltasauridae and Colossosauria, as well as differences between members of non-colossosaurian, non-lithostrotian Titanosauria and Colossosauria and members of non-lithostrotian Titanosauria and Saltasauridae. The test of LD2 of the humeri also found significant differences between members of Lithostrotia and non-lithostrotian Titanosauria, but no significant differences between members of Colossosauria and Saltasauridae along LD2. The test of LD1 of the ulnae found significant differences among all the analysed clades except for the members of Aeolosaurini and Colossosauria and members of Colossosauria and Lithostrotia. In contrast, LD2 of the ulnae recovered significative differences between members of Colossosauria and Lithostrotia as well as between members of Colossosauria and Saltasauridae. The test of LD1 of the radii found significant differences among Colossosauria, non-saltasaurid Lithostrotia and Saltasauridae. LD1 of the femora highlights significant differences among Colossosauria, non-lithostrotian Titanosauria, Saltasauridae and between members of Saltasauridae and non-saltasaurid Lithostrotia and between members of non-lithostrotian Titanosauria and Lithostrotia. In contrast, significant differences were found along LD2 of the femora between members of Colossosauria and Lithostrotia, between members of Colossosauria and Saltasauridae, and between members of Lithostrotia and non-lithostrotian Titanosauria as well as between members of Saltasauridae and non-lithostrotian Titanosauria. LD1 of the tibiae recovered significant differences between members of Saltasauridae and Colossosauria and between members of non-saltasaurid Lithostrotia and Saltasauridae. Lastly, LD1 of the fibulae recovered significative differences between members of Colossosauria and Lithostrotia, members of Colossosauria and Saltasauridae and members of non-saltasaurid Lithostrotia and Saltasauridae. LD2 of the fibulae highlights significative differences in the comparison of members of Colossosauria and Saltasauridae and members of non-saltasaurid Lithostrotia and Saltasauridae.

A secondary run of both tests was also made, comparing pair-wise the different operative taxonomic units to which the analysed specimens belong for both the PCA and LDA results of all the element types. These analyses can also be accessed in Online Resource 3.

3.3 High density surface semilandmarks

Surface semilandmarks were analysed through LDA using the same methods as used to examine morphologic trends based on the landmark with semilandmark curves dataset. The results are also similar to those obtained from the analyses of the landmarks and semilandmark curves dataset. A comprehensive report of these results can be accessed in Online Resource 3 and we briefly summarize them here. The LDs were used to calculate Procrustes distances between surface semilandmarks the morphology exhibited in the most negative and positive values in each LD in order to identify the bone regions which account for most of the between group differences outlined by the above analyses.

The humeral high-density semilandmarks indicate that most of the variance along LD1 is found in the extent protrusion of the medial corner of the proximal end (Fig. 7a). Another of the regions which also account for a high variation is the morphology of the lateral corner of the proximal end in anterior view, the anteroposterior development and mediolateral breadth of the deltopectoral crest, and the anteroposterior development of the entepi- and ectepicondyle in the distal end (Fig. 7a). In contrast, the posterior face of the distal end only exhibits variance in the morphology of the medial margin and the distal part of the ridges that surround the anconeal fossa and connects with the medial and lateral condyles (Fig. 7a). LD2 identifies more subtle patterns of variation with most of the changes occurring along this axis representing variation in the shape of the lateral corner of the proximal end in anterior view and the morphology of the medial and lateral margins of the distal end (Fig. 7b).

The ulnae exhibit considerable variance along LD1 concentrated in the morphologies of the anteromedial, posterolateral and olecranon processes (Fig. 7c), especially in the olecranon and anteromedial processes in that order. There is also subtle variance along LD1 in the form of the distal portion of thearticulation with the radius in the anterior face

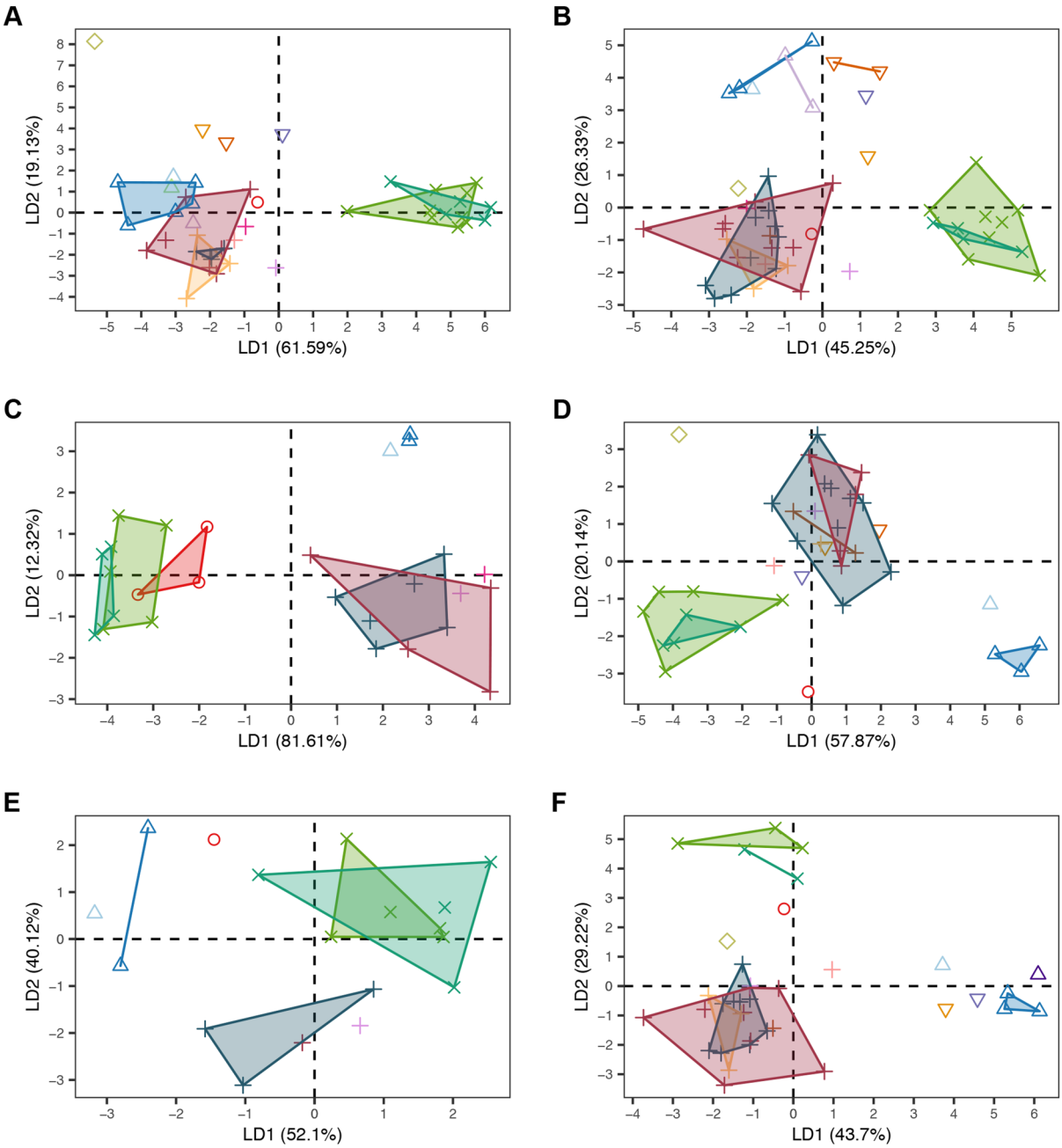
A
LD2 (19.13%)
LD1 (61.59%)
B
LD2 (26.33%)
LD1 (45.25%)
C
LD2 (12.32%)
LD1 (81.61%)
D
LD2 (20.14%)
LD1 (57.87%)
E
LD2 (40.12%)
LD1 (52.1%)
F
LD2 (29.22%)
LD1 (43.7%)
Clade
Aeolosaurini
Colossosauria
Lithostrotia
Saltasauridae
Somphospondyli
Titanosauria
OTU
Aeolosaurus
Antarctosaurus
Argentinosaurus
Bonatitan
Bonitasaura
Elaltitan
Jainosaurus
Ligabuesaurus
Lirainosaurus
Morphotype I
Morphotype II
Mendozasaurus
Muyelensaurus
Narambuenatitan
Neuquensaurus
Notocolossus
Petrobrasaurus
Rinconsaurus
Saltasaurus

◂**Fig. 6** LDA results over the GPA aligned landmark and semilandmark curves of the fore- and hindlimb skeletal elements. LDA of the sample of humeri (**a**), LDA of the sample of ulnae (**b**), LDA of the sample of radii (**c**), LDA of the sample of femora (**d**), LDA of the sample of tibiae (**e**) and LDA of the sample of fibulae (**f**). *OTU* operative taxonomic unit/morphotype. Shape and color legend indicated in the bottom of the image

of the distal end (Fig. 7c). LD2 primarily characterizes the variance in the morphology of the olecranon process in the posterior face (Fig. 7d). There are also morphological differences along LD2 in a small area around the medial corner of the distal end (Fig. 7d).

Concerning the radii, we found that most of the variance along LD1 to represent differences in the form of the lateral and medial corners of the proximal end especially in anterior view (Fig. 7e). Additional variation along LD1 occurs in the shape of the medial corner of the distal end (Fig. 7e). Lastly, there are some subtle variations in the shape of the interosseous ridge (Fig. 7e). LD2 characterizes variations in the morphology of the medial and lateral corners of the proximal end (Fig. 7f). However, unlike LD1, LD2 also captures the variation in the morphology of the proximal to proximomedial portion of the posterior face, proximal to the interosseous ridge (Fig. 7f). Other areas exhibiting considerable variance along LD2 include the robusticity of the medial and lateral corners of the distal end, including the surface surrounding the pmdc (Fig. 7f). There is also subtle variation in the shape of the region just proximal to the posteromedial distal condyle (Fig. 7f).

Analyses of the femora found most of the variance along LD1 reflects the extension of the lateral bulge off the shaft of the bone (Fig. 8a). More subtle differences occuring along this LD include variations in the overall morphology of the femoral head, especially its posterodorsal portion; and in the posterior form of the tibial (Fig. 8a). The posterior face of the fibular condyle also exhibits subtle variation along this LD. LD2 captures variations in the shape of the posterior outline of the femoral head and the posterior morphology of the fibular condyle (Fig. 8b). In general, the rest of the surface area of the femur as captured by both LDs exhibits much less variation than in the other limb elements analysed (see Figs. 7, 8).

The tibiae primarily exhibit variations in the form of the proximal end, especially of the anteromedial edge, in the medial area of the fibular articulation and the posteromedial edge (Fig. 8c). Other areas exhibiting considerable variation surround the distal end, concentrated in the form of the articular surface for the ascending process and the medial surface of the distal end, with the posterodistal process being comparatively less variable (Fig. 8c). The LD1 does not capture much variation in the morphology of the cnemial crest. However, LD2 highlights most of the variation in the shape of the cnemial crest, especially in the distal portion that descend to the muscular attachment surfaces for the *Mm. femorotibiale* and *ambiens* (following Otero and Vizcaino 2008; see Fig. 8d). The second most variable area along LD2 is the posterior face of the proximal end, especially toward the lateral side of this face (Fig. 8d). The lateral surface of the tibia and its region for the articulation with the ascending process of the astragalus exhibit only slight variations in form along this LD (Fig. 8d). However, these variations are quite subtle in comparison with the other regions characterized by LD1.

The fibulae exhibit few differences along LD1, with most variation occurring in the posterodistal curvature of the shaft distal to the lateral trochanter; these variations also wrap around the posterior face (Fig. 8e). LD1 also captures variation in the relative protrusion of the anterior trochanter (especially in anterolateral view), the shape of the distal end and the anterolateral crest (Fig. 8e). These differences however, are subtle in comparison with those evident in the morphology of the shaft (Fig. 8e). LD2 in contrast, highlights most of the differences in the shape of the proximal end, especially in its posterolateral and posterior portions (Fig. 8f), and minor differences in form near the area of the anterior trochanter. This LD also captures subtle variations in the shape of the laterodistal surface of the distal portion of the shaft, the distal articular surface, and the posteromedial portion of the distal end (Fig. 8f).

4 Discussion

4.1 Morphospace occupation by titanosauria

Most of our analyses of sample variance via PCA show similarities in the general morphology of the entire non-autopodial limb skeleton of the majority of the sampled titanosaurs. This is congruent with previous findings in the analysis on humeri and femora that also included representatives of Titanosauria (Ullmann et al. 2017). Saltasauridae is the only titanosaurian clade found to occupy separated morphospaces from other titanosaurian clades, at least for the entire non-autopodial appendicular skeleton (e.g. Figs. 4, 5). There are some taxonomically-meaningful morphological differences among the analysed taxa (e.g. separation of some taxa by the extreme gracility of the tibia, PC1: Fig. 5c, d). Nevertheless, for most of the analysed appendicular elements these differences pertain to particular taxa or morphotypes (i.e. Morphotype II at Lo Hueco with a gracile tibia, Fig. 6c) there are no clearly visible differences among more exclusive titanosaurian clades (following current phylogenetic hypotheses of Gonzalez Riga et al. 2018, 2019; Mannion et al. 2019). In the case of saltasaurids, not all their elements of the limb skeleton are clearly different from those of other sauropod clades (e.g. saltasaurids do not occupy

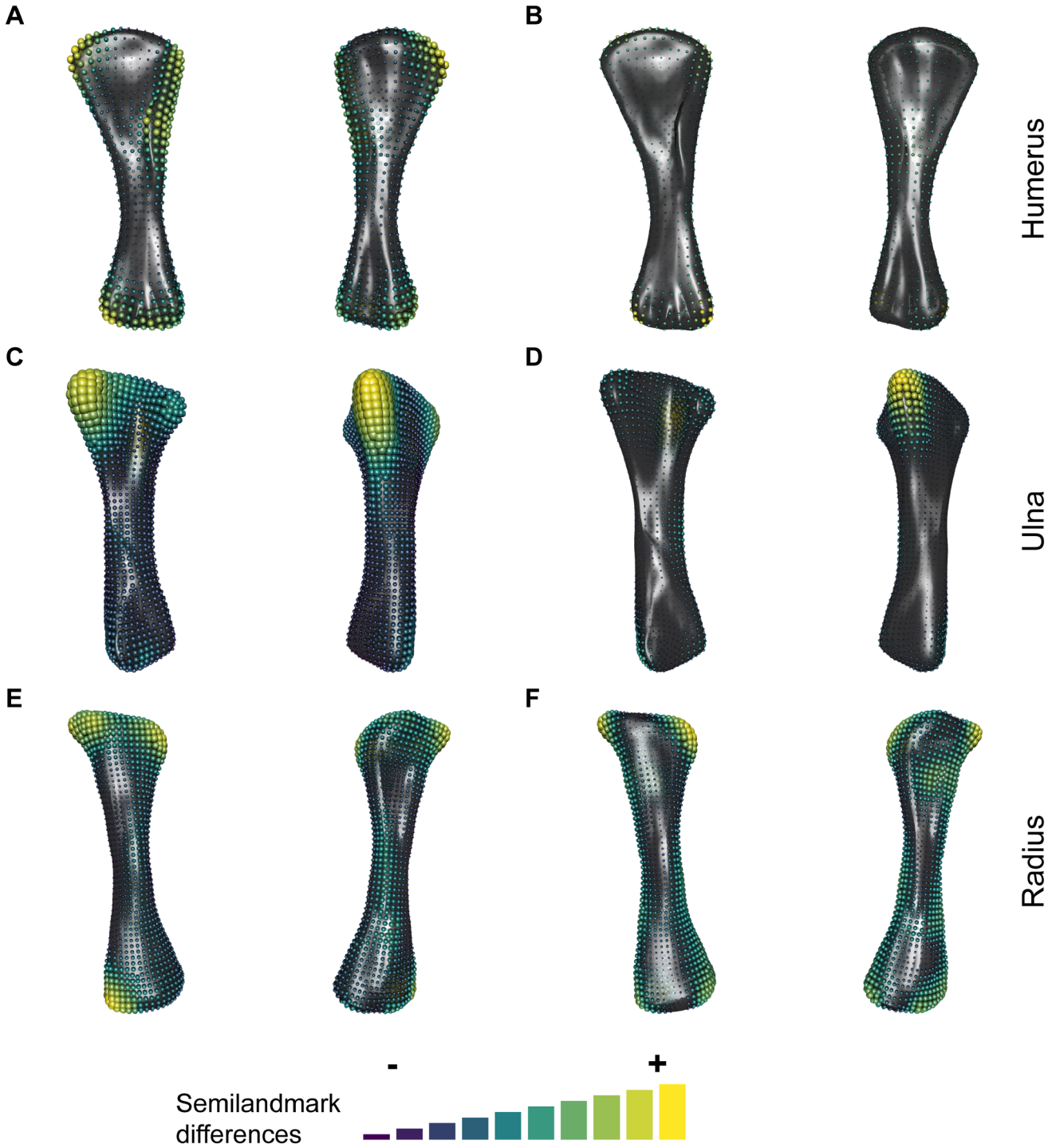

Fig. 7 Intra-landmark Procrustes distances derived from LDA of high-density surface semilandmarks distributed across each forelimb stylopodial and zeugopodial element. Areas with largest differences on LD1 of the humerus in anterior and posterior views (**a**), areas with largest differences on LD2 of the humerus in anterior and posterior views (**b**), areas with largest differences on LD1 of the ulna in anterior and posterior views (**c**), areas with largest differences on LD2 of the ulna in anterior and posterior views (**d**), areas with largest differences on LD1 of the radius in anterior and posterior views (**e**), and areas with largest differences on LD2 of the radius in anterior and posterior views (**f**). Size and color scale proportional to × 2 Procrustes distances

Table 5 Kruskal Wallis over the shape LDs; χ^2 and p values after Bonferroni correction

	Humerus		Ulna		Radius		Femur		Tibia		Fibula	
	Chi-sq	p value	Chi-sq	p value	Chi-sq	p value	Chi-sq	p value	Chi-sq	p value	Chi-sq	p value
LD1	34.770	0.000*	20.325	0.001*	11.303	0.041*	33.999	0.000*	26.794	0.001*	18.788	0.034*
LD2	27.414	0.000*	9.742	0.084	10.887	0.049*	26.182	0.000*	27.081	0.001*	18.839	0.033*
LD3	9.723	0.501	8.342	0.158	3.453	1.000	10.810	0.332	12.660	0.428	17.147	0.068
LD4	20.976	0.005*					20.670	0.006*	11.027	0.814	8.933	1.000
LD5	17.596	0.021*					10.070	0.440	5.515	1.000	4.478	1.000

$\alpha = 0.05$, significant p values indicated with '*'

a unique morphospace for either the radii or the fibulae, Fig. 4e, f, 5e, f). However, this lithostrotian clade does possess a distinctively robust appendicular skeleton overall which clearly occupies a distinct morphospaces for most of the limb elements studied. Among the other somphospondylans analysed, only the colossosaurs exhibit an isolated humeral and slightly different ulnar PCA morphospaces occupation compared with the regions occupied by other sauropod clades (Fig. 4a). Some colossosaurian humeri are recovered among some of the most gracile elements included in our analyses (e.g. *Muyelensaurus pecheni*), which can be observed by them plotting slightly apart from other taxa on both the PC1 and PC2 (Fig. 4a).

Identification of extensive morphological similarities between such distinct titanosaurian clades is not unheard of (Ullmann et al. 2017; see Bonnan 2004, 2007 for other neosauropod clades). The appendicular skeleton of many titanosauriforms has been previously analysed using GMM and many morphological similarities between different taxa both within the same clade and between distinct clades were reported (Ullmann et al. 2017). When maximizing differences between groups via LDA, we found differences between the titanosaurian morphospace and that occupied by the non-titanosaurian somphospondylans, represented solely by *Ligabuesaurus leanzai* in this study. Our findings are congruent with those of previous studies that found separation between early-branching titanosauriforms and titanosaurs (Ullmann et al. 2017). The humerus, tibia and fibula of *Ligabuesaurus leanzai* clearly plot apart from other titanosaurian specimens in the LDA morphospaces (Figs. 5b, 7d, f). However, the femur of this taxon is very similar to those of other titanosauriforms (Fig. 7b). Previous GMM analyses on the autopodial elements of sauropods including both non-titanosaurian titanosauriforms and titanosaurs found similar trends in separation of the humeri but lesser shape differences among sauropod femora (Ullmann et al. 2017).

We also found differences in morphology between the more gracile colossosaurian forelimb elements and those of other titanosaurs (Figs. 4, 5, as commented above). Some authors have suggested that more gracile and elongated forelimb elements may be related to a more anteriorly-displaced Center of Mass (following Henderson 2006; Bates et al. 2016; Ullmann et al. 2017). Previous analyses of the morphology of the sauropod stylopodium reported similar convergence between the gracile humeri of *Paralititan stromeri*, *Muyelensaurus pecheni, Brachiosaurus altithorax* and *Giraffatitan brancai* (Ullmann et al. 2017). This distinct morphospace occupation for several of the analysed elements implies differences concerning the posture of the animal, which could be related to distinct ecomorphological traits in comparison with other titanosaurs rather than phylogenetic affinities (Henderson 2006; Christian et al. 2011; Ullmann et al. 2017). The colossosaurian humeri are clearly unique, occupying a separate morphospace from the gracile elements of other members of Titanosauria (Fig. 4a, b). In contrast, the forelimb zeugopodium exhibits a slightly slenderer morphology that resembles and therefore overlaps with the morphospace region of other titanosaurs (Fig. 4c, f). It is also relevant that the ulnae of some colossosaurs share similarities with other slender ulnae, namely those of *Mendozasaurus neguyelap* and Morphotype II at Lo Hueco which overlap in a similar PCA morphospace region (Fig. 4).

Our analysis of the hindlimb morphospace found an overlap among all non-saltasaurid somphospondylans. Non-saltasaurid titanosaurs do not present major differences in the overall morphology (Fig. 5). However, subtle differences can be seen between the morphospace occupation of colossosaurians and other non-colossosaurian titanosaurs (e.g.. differences between colossosaurian and non-colossosaurian femora and tibiae on PC2, Fig. 5a, c) in all the hindlimb elements analysed.

Such morphospace overlapping among such varied titanosaurian clades supports the previous hypotheses of morphological resemblance in limb posture being due to distinct ecomorphological traits rather than phylogenetic affinities (Ullmann et al. 2017). The LDA, however, allowed recognition of differences among most of the analysed somphospondylans when the between-group differences are maximized (Fig. 6). The members of Colossosauria were recovered isolated from other titanosaurian clades for each analysed appendicular elements (Fig. 6) and were often found to be plotted closer to lithostrotian forms than to non-lithostrotian

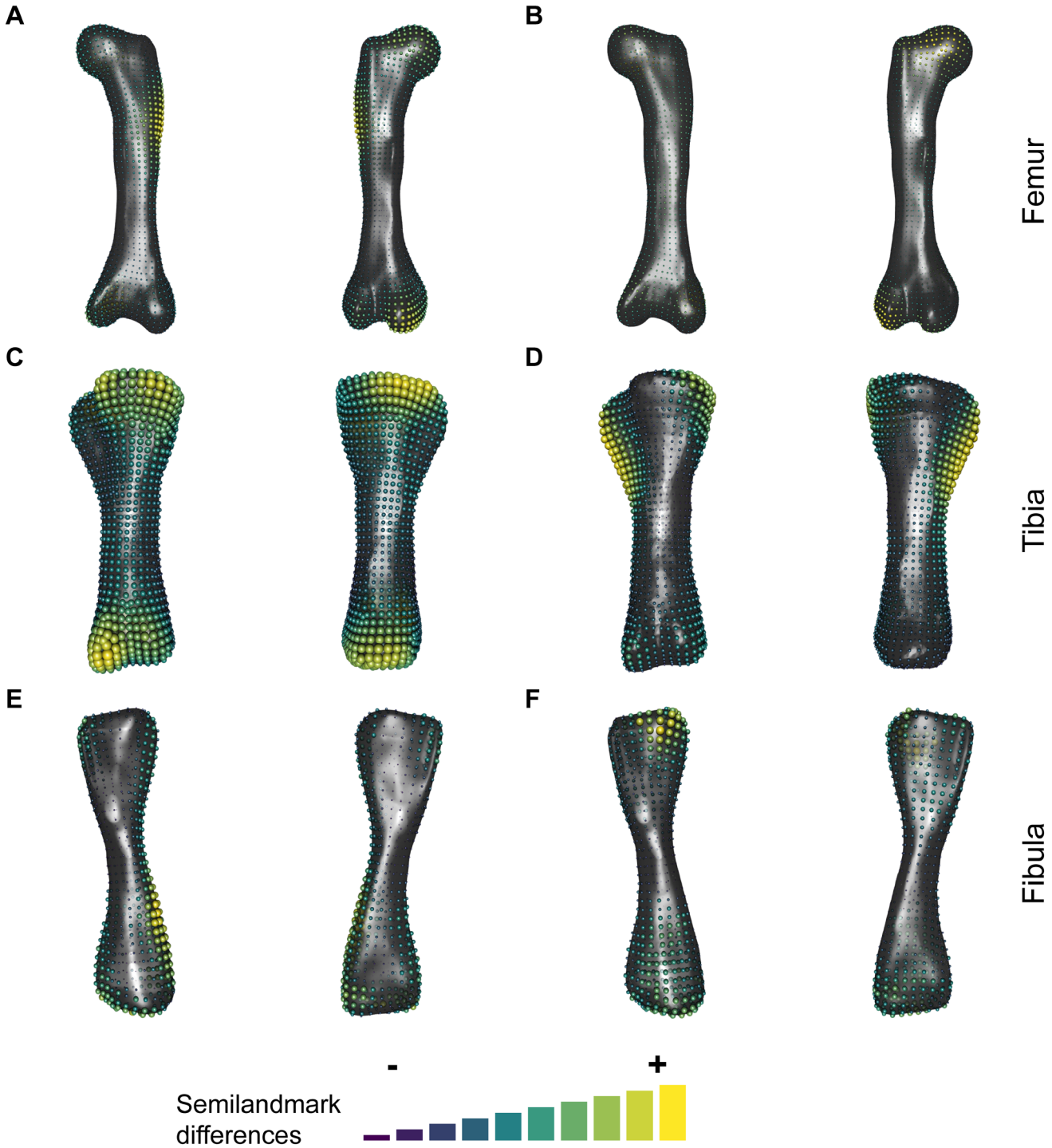

Fig. 8 Intra-landmark Procrustes distances derived from LDA of high-density surface semilandmarks distributed across each hindlimb stylopodial and zeugopodial element. Areas h largest differences on LD1 of the femur in anterior and posterior views (**a**), areas with largest differences on LD2 of the femur in anterior and posterior views (**b**), areas with largest differences on LD1 of the tibia in anterior and posterior views (**c**), areas with largest differences on LD2 of the tibia in anterior and posterior views (**d**), areas with largest differences on LD1 of the fibula in anterior and posterior views (**e**), and areas with largest differences on LD2 of the fibula in anterior and posterior views (**f**). Size and color scale proportional to × 2 Procrustes distances

titanosaurians. However, the PCA highlights less and more subtle morphological differences between the specimens of the different analysed clades, therefore the variation may be related to ecomorphological traits, as suggested in previous studies (Henderson 2006; van Buren and Bonnan 2013; Ullmann et al. 2017). Our LDA was nevertheless capable of identifying taxonomically-relevant patterns in the morphospace occupation because it consider the within-group variance and maximizes the intergroup variance along each linear discriminant (see Claude 2008).

Our LDAs found separation of the morphospace occupation of colossosaurs from other non-lithostrotian titanosaurians (Figs. 5, 7). Moreover, non-colossosaurian titanosaurs and the non-saltasaurid lithostrotians present similar morphospace occupation in our LDAs. In particular, Rinconsauria often occupies the most distinct region of the Colossosauria unique morphospace compared to other colossosaurs and non-colossosaurian titanosaurs in most of our LDAs (Figs. 5, 7). The separation for all the elements via LDA (Figs. 5, 7) contrasts with the morphological differences in the humeri identified by our PCA. While there are morphological convergences with other gracile lithostrotians in the femora and the zeugopodial elements of both limbs (see Figs. 4, 6), it is possible that Rinconsauria, as an early-branching member of Colossosauria, may have occupied a new and distinct limb morphospace compared to other early-branching non-colossosaur titanosaurs (see the isolated region of humeral and ulnar PCA morphospace, Fig. 4a, c; see partially isolated region of tibial PCA morphospace, Fig. 5c). In particular, Rinconsaurs appear to exhibit a unique forelimb morphology that retains morphofunctional similarities to other gracile titanosaurs only to some extent (proximity of other lithostrotian specimens in the PCA morphospace, Figs. 4, 5), and will translate into a particular combination of osteological characters. It appears this new morphospace was subsequently exploited by more deeply-nested colossosaurs (e.g. *Mendozasaurus neguyelap*, exhibits more similarities with other lithostrotians for some elements, *Notocolossus gonzalezparejasi* and *Argentinosaurus huinculensis*, exhibit similar morphology to other titanosaurs), which are in comparison morphologically more similar to other non-colossosaurian titanosaurians as suggested by our PCAs (Fig. 4a). However the specimens of deeply-nested colossosaurs plot more separated from other non-colossosaurian titanosaurs when the between-group differences are considered in our LDAs (Fig. 6a). Morphological convergence between taxa from distantly-related sauropods clades, such as the colossosaur *Mendozasaurus neguyelap* and lithostrotian Morphotype II at Lo Hueco, suggests an achievement of similar ecomorphological adaptations (see overlapping in the regions of the ulnar and tibiae PCA morphospaces, Figs. 4c, 5c). Also, other non-rinconsaurian colossosaurs present a more primitive morphology in their elements (e.g., humerus of *Notocolossus gonzalezparejasi*, González Riga et al. 2016, 2019) similar to other titanosaurians as they plot in a proximate region of the morphospace of our PCAs(see the plotting position of *N. gonzalezparejasi* case above, see also the plotting position of the fibula of *Argentinosaurus huinculensis*, Figs. 4a, 5e) and therefore these deeply-branched colossosaurs will present some character scorings more similar to more early-branching titanosaurs. However, when the clade-level morphospaces are compared by maximizing the differences via LDA, all the specimens of Colossosauria occupy the same isolated area of the morphospace (i.e. Fig. 6b, f), and all our LDAs plot the rinconsaurs in the most separated portion of the colossosaurian morphospace compared to the region occupied by other non-colossosaurian titanosaurs. Following the phylogenetic hypothesis of Gonzalez Riga et al. (2019) these LDA results suggest an acquisition of apomorphic morphology (Figs. 4, 5, 6) in colossosaurs which became especially gracile and unique (especially the forelimb) in Rinconsauria (e.g. Fig. 6a–d). This condition is slightly reverted to more primitive morphology in more deeply-branching colossosaurs (e.g. *Notocolossus gonzalezparejasi* humerus Fig. 6a, b). In contrast, the non-saltasaurid lithostrotians present a more plesiomorphic morphology similar to that of more early-branching non-colossosaur lithostrotians following the phylogenetic hypothesis of Gonzalez Riga et al. (2019). It is also important to note that these patterns are regionalized within the colossosaur limb skeleton, as the femur exhibits a more plesiomorphic morphology, overlapping with other lithostrotian taxa in the PCA morphospace (Fig. 5a) and closer to the LDA morphospace region occupied by non-lithostrotian titanosaurs (Fig. 6d).

Saltasaurids were found separated apart from the morphospaces of other titanosaurian clades in most of our PCAs and LDAs. Following our previous hypothesis that the morphological similarities in our PCAs reflect most likely the acquisition of similar ecomorphological traits, saltasaurids exhibit an entirely distinct morphology. Members of this clade occupy morphospace locations isolated and indicative of a unique posture in almost all our analyses (see comparison among the PCAs and LDAs Figs. 4, 6). Many previous studies have included representatives of saltasaurids as a template of the titanosaurian body plan, partly based on the availability of skeletal material at that time (e.g. Salgado et al. 1997; Sanz et al. 1999; Wilson 2002; Upchurch et al. 2004; but see observations made by Powell 2003, and the inclusion and analysis of other titanosaurian taxa by Curry Rogers 2005). These results suggest that saltasaurids rather than exhibiting a general titanosaurian (or more exclusively lithostrotian) body plan, acquired an unique appendicular morphology probably related to a extreme development of "wide-gauge" posture (see Figs. 5, 6). This unique configuration may presumably be also responsible for the abrupt shift of the Centre of Mass toward a more posterior position

within the torso suggested in previous studies (Bates et al. 2016). Inclusion of other titanosaurian taxa in such analyses is important in order to better understand previously-undescribed and underrepresented taxa (González Riga et al. 2019). It is also noteworthy that the saltasaurid appendicular skeleton represents a highly specialized and derived morphology, distinct from that of other known titanosaurian clades. These statements are supported in our analyses as the analysis of the autopodial elements of the member of this clade are isolated in the PCAs whereas other non-saltasaurids overlap in the morphospace. Therefore the saltasaurids are the single clade which plot in an isolated region of the PCA morphospace reflecting unique posture differences due to both ecomorphological adaptations and phylogenetic affinities for most of the performed analyses (Figs. 5, 7).

4.2 Osteological character implications

The phylogenetic position of Titanosauria and its definition have been supported mainly by axial synapomorphies while the appendicular skeleton has played a secondary role (e.g. Wilson 2002; Upchurch et al. 2004). However, we found slight morphological differences among titanosaurian clades in the exploratory analyses (PCA; Figs. 4, 5) that can be used to discuss some features of those elements (e.g. the morphology of the lateral corner of the proximal end of the humerus; Fig. 4a, b). In addition, use of LDA takes into account morphological variability within the a priori defined in-group relationships (e.g. among members of Colossosauria, Lithostrotia, etc.). This morphological variability includes intraspecific variability within the same taxon or morphotype (e.g. wide variability in the morphology of ulnae of *Saltasaurus loricatus*, Fig. 4; also see Páramo et al. 2016, 2018, for intraspecific variability among the titanosaurians from Lo Hueco). After initially characterizing within-group variation, the algorithm then defines each linear discriminant by maximizing the between-group differences (e.g. disparity between Titanosauria and the more exclusive clade Lithostrotia). The results of our LDA therefore highlight distinct morphological differences that can be relevant to phylogenetic analyses, as the identified differences stem from separation between exclusive clades within Somphospondyli (see also the analyses using this algorithm in Ullmann et al. 2017). The morphological variation highlighted in our results has already been incorporated in some of the proposed phylogenetic characters. However, other osteological characters may need some modifications in the light of our results and there is the possibility that some of the variations could translate in future new character(s). A comprehensive list of the phylogenetic characters can be accessed in Table 6, which includes some already established morphological characters that should be the focus of future recodifications as well as other morphological variations that are still not considered in the available data sets.

Most of the differences in LD1 on the humeri are related to the morphology of the medial corner of the proximal end, the form of the proximolateral margin and the deltopectoral crest, and the morphology of the distal end (Fig. 7a). The shape of the lateral corner of the proximal end as well as the length and projection of the deltopectoral crest are already incorporated into several osteological characters in common use (Sanz et al. 1999: Ch35; Wilson 2002: Ch159; Upchurch et al. 2004: Ch217 and Ch218; see discussion on Ch225 in Harris 2006; also see more recent works by Carballido et al. 2017; Mannion et al. 2019). The morphology of the medial corner of the proximal end is already incorporated into several characters associated with the overall morphology of the proximal end such as the shape of the proximal profile in anterior view (González Riga 2003: Ch26 and Ch27; Gorscak et al. 2017: Ch191). Another osteological character in the morphology of the proximal end has been used as well, which is focused on the shape of the union between the profiles of proximal and lateral margins (Mannion et al. 2013: Ch223). However, observation of simple differences between a squared or more-rounded morphology may not be enough to adequately describe the medial portion of the proximal end of some specimens which preserve a more complex morphology, as some authors have previously pointed out (e.g. Harris 2006). For example, the squared proximal morphologies of Morphotype II at Lo Hueco, (e.g. HUE-1643) and *Lirainosaurus astibiae* (e.g. MCNA-7463) also exhibit asymmetry owing to medial deflection of the humeral head. This asymmetrical, squared proximal morphology does not resemble the morphology of *Saltasaurus loricatus*, which exhibits a more saddle-shaped proximal outline (e.g. PVL-4017–69). Further work is needed to test if this morphological distinction is useful as a potential new character. Recent works have proposed two additional characters related to the proximomedial corner of the humerus. One of these characters (Tschopp et al. 2015: Ch384; see also Ch364 in Poropat et al. 2016) attempts to codify differences in the medial projection of the proximal end, as exemplified in this study by the humeri of *Muyelensaurus pecheni* (e.g. MAU-PV-132) and Morphotype II at Lo Hueco (Fig. 4a). The other character refers to relative development of the convexity of the curvature between the corners of the proximal end and the extent of development of the proximolateral corner of the deltopectoral crest, producing either the apomorphic "hourglass" sauropod morphology (e.g. Morphotype I of Lo Hueco specimen HUE-817) or the more asymmetrical profile of many titanosauriforms (e.g. *Mendozasaurus neguyelap* specimen IANIGLA-69-1; Ch365 in Poropat et al. 2016; Mannion et al. 2019).

Other areas of the humerus exhibiting considerable morphological variation are the ridges of the supracondylar

Table 6 Morphological osteological characters relatable to the morphological variability found in the LDA on the surface semilandmarks

Element	Morphological variation	Characters
Humerus	Shape of the profiles of the union between the humeral proximal end medial and lateral margins	Cb260; CR271; DE79; Mn223; S94
	Asymmetrical morphology of the humeral proximal outline	Ma172; Mn224; P364-365; P384; T384
	Medial corner of the humerus distal end / development of the ectepicondyle	C186; CR272-273; H231; M517; W163; This study*
	Posterior *M. deltoideus clavicularis* tuberosity and *M. latissimus dorsi* tuberosity	M226; P367
Ulna	Depth of anterolateral concavity in proximal view	Cb261; H234; M281; U223; Up173; W165; WS5
Radius	Bevelling of the distal end with or without proximal curvature of the shaft	Cb267; CR289; DE87; H246; M49; P371; T393
	Posteromedial distal ridge	This study*
	Posterior to posterolateral concavity of the surface of the shaft under the proximal end	This study*
Femur	Anteroposterior width of the lateral bulge	This study*
	Anterior deflection of the lateral bulge	This study*
	Anteroposterior width of the distal condyles	M535; P389; RT171; Wh179; This study*
	Orientation of the lateral epicondyle	This study*
Tibia	Accessory fibular articulation posterolateral ridge in the proximal end, posteriorly to the second cnemial crest	RT180; This study*
	Rotation of the distal condyles of the tibia	Sz42
	Morphology of the distal portion of the cnemial crest	M536; RT177; T444
Fibula	Morphology of the anterior trochanter and the proximal end	DE111; Mn262; T447; RT unnumbered character
	Lateromedial torsion of the anterolateral crest in the distal end	P394, M394

Cb—Carballido et al. (2012); C—Carballido et al. (2017); CR—Curry Rogers (2005); DE—D'Emic (2013); H—Harris (2006); Ma—Mannion et al. (2012); Mn—Mannion et al. (2013); M—Mannion et al. (2019); P—Poropat et al. (2016); RT—Royo-Torres et al. (2009); S—Sereno et al. (2007); Sz—Sanz et al. (1999); U—Upchurch et al. (2004); Up—Upchurch et al. (2007); Wh—Whitlock (2011); W—Wilson (2002); WS—Wilson and Sereno (1998). This study*—indicates that the exact morphological variation is not found in any current osteological character definition (see text)

area of the distal end which delimit the anconeal fossa in posterior view, the lateral distal condyle in anterior view, and the shape of the medial margin of the humerus. The development of supracondylar ridges surrounding the anconeal fossa are osteological features previously considered in phylogenetic characters (Sanz et al. 1999: Ch36; Upchurch et al. 2004: Ch221). The projection of the lateral anterior distal condyle in the anterior face is also incorporated into an osteological character in a recent study (Poropat et al. 2016: Ch351); our observations are congruent with their character definition, and no further characters areneeded to capture this variance. However, the morphology of the medial corner of the distal end has not been considered by any osteological character beyond those summarizing the overall distal expansion of the humerus (e.g. Curry Rogers 2005: Ch272 and Ch273). In particular, Morphotype II at Lo Hueco, *Lirainosaurus astibiae*, and some elements from *Muyelensaurus pecheni* exhibit marked differences in development of the humeral ectepicondyle. The ectepicondyle is more robust in saltasaurids, forming a shallower concavity and causing the absence of a ridge-like margin (e.g. MLP-CS-1479). Our results indicate that the shape of this portion of the humerus exhibits enough variation to warrant relevance as a new osteological character.

The region posterior to the deltopectoral crest also exhibits some variation across both LD1 and LD2 (Figs. 5a, 7a, b). This variation is partly captured by a character describing the insertion of the *M. latissimus dorsi* (D'Emic 2012; for locations of muscular insertions, see Otero 2018; also Ch226 in the morphological dataset of Mannion et al. 2013). However, there is also a secondary posterior ridge present in several titanosaurian taxa (e.g. *Lirainosaurus astibiae*, both morphotypes from Lo Hueco). Previous myological studies have identified the *M. latissimus dorsi* as one of the major extensor muscles attaching to the posterior proximal portion of the humerus in crocodiles and sauropodomorphs. This attachment can be related (when it is not a fleshy insertion) by a ridge located posterolateral to the deltopectoral crest (e.g. *Opisthocoelicaudia skarzinskii*: Borsuk-Bialynicka 1977; in *Mussaurus patagonicus* and *Zby atlanticus* Otero 2018 and in *Dreadnoughtus schrani* Voegele et al. 2020). Additionally, this ridge could also house the attachment area of the *M. teres major*, though its presence is equivocal in sauropodomorph dinosaurs (or all non-avian dinosaurs; see Remes 2007 contra Otero 2018 and Voegele et al. 2020). The other region that exhibits variation is the ridge or tuberosity posterolateral to the deltopectoral crest, which has been noted previously (D'Emic 2012) and included in

an osteological character (Ch367 in Poropat et al. 2016). However, this osteological feature only describes the presence or absence of a ridge as the osteological correlate for the attachment of the *Mm. deltoideus clavicularis* as well as the lateral margin of the lateral triceps fossa (sensu Poropat et al 2016). The arrangement of the different muscles attaching to this region is complex, sometimes the insertion of the *M. latissimus dorsi* is assigned to a tuberosity laterally placed (e.g. *Zby atlanticus* and *Opisthocoelicaudia skarzinskii*, as noted above) or a ridge (*Rapetosaurus krausei*, Otero et al. 2018: Fig. 7). However, some titanosaurs alternatively exhibit a rugosity in the middle of the posterior face at this same proximodistal position (*Lirainosaurus astibiae*, see Díez Diaz et al. 2013; Morphotype II specimen HUE-3228 and *Dreadnoughtus schrani*, Voegele et al. 2020). Other titanosaurs do not exhibit a ridge for the *M. latissimus dorsi* attachment but present some variation in the posterior tuberosities of the deltopectoral crest. Some titanosaurs present a posterolaterally *M. deltoideus scapularis* ridge, and possibly in some taxa also the *M. scapulohumeralis* ridge (e.g. *Dreadnoughtus schrani*, Voegele et al. 2020), that is visible in the lateral margin in anterior view (e.g. specimen PVL-4017-62 referred to *Saltasaurus loricatus* and specimen MCF-PHV-233-10 referred to *Ligabuesaurus leanzai*). However, other titanosaurs exhibit a shorter posterior ridge, with no continuity to the posterolateral corner of the deltopectoral crest, and no *M. latissimus dorsi* ridge (specimen PVL-4628 referred to *Elaltitan lilloi*). It is also important to note that the posterior ridge which is the attachment for the *M. latissimus dorsi* may also pertain to the attachment of the *M. teres major*, but it is difficult to assess this, as it rarely leaves osteological correlates in Dinosauria (Remes 2007; Piechowski and Tałanda 2020; Voegele et al. 2020). We consider that the current definition of the character referring to the posterior ridge of the deltopectoral crest (Ch367 in Poropat et al. 2016) does not include all the complexity in the muscular attachments within this region, the variation in the projection between more posterolateral and posterior ridges or tuberosities, and therefore all of the resulting morphological diversity. For the moment, our analyses found that most between-group variability in this region extends beyond the *M. deltoideus clavicularis* insertion tuberosity, but we feel that no further modification can be proposed to the existing character given the current sample size.

Most of the variance in the ulna is found mainly in the three processes of the proximal end (Fig. 7c, d). Variations in the angle between the anteromedial and posterolateral processes have already been incorporated into an osteological phylogenetic character (Tschopp et al. 2015: Ch389). The relative size of each process has also been used as a character (D'Emic 2012: Ch85, after Wilson 2002), and our results are congruent with recent characters describing the position of the anteromedial process (Ch51 of the morphological character dataset of González Riga et al. 2018) and the depth of the concavity along the articulation with the humerus in the proximal view (Mannion et al. 2013: Ch235). These morphological differences were found in our analyses (Figs. 4c, d, 5c, d) between the more concave and dorsally projected anteromedial process of *Rinconsaurus caudamirus* (MAU-PV-N-425) and *Muyelensaurus pecheni* (MAU-PV243) and the slightly less concave and straighter anteromedial process of *Saltasaurus loricatus* (PVL-4017-72). There is also considerable variability in the form of the olecranon process in both LD1 and LD2 (Fig. 7c, d). This variance can be related to the differences between the robust and mediolaterally-wide posterior portion of the vault-shaped olecranon process in Saltasauridae and Aeolosaurini versus the slightly posteriorly-projected and mediolaterally-narrow posterior portion of the olecranon process in other titanosaurs (along LD1, Fig. 6b). There are also same-clade differences in the posteriorly-projected and slightly curved olecranon process among colossosaurian sauropods as in *Mendozasaurus neguyelap* (IANIGLA-70-1) and *Muyelensaurus pecheni* (MAU-PV-72). This variability has been recently included in osteological phylogenetic matrices (Ch281 in the morphological character dataset in Mannion et al. 2019 after Upchurch et al. 2015) although it might need to be revised to include differences between the "Y-shaped" morphology and "T-shaped" morphology, including the depth of the anterolateral concavity in proximal view observed here.

We also observed some subtle variations in the morphology of the radial articulation near the distal end of the ulna (Fig. 8c). This variation has been captured by a phylogenetic character describing to the distal end and articular surface morphologies (Curry Rogers 2005: Ch280). No further character definition is needed for that character to code the variability observed in our analyses.

Most of the variation observed among the analysed radii occurs in the shape of the medial and lateral corners of the proximal end (Fig. 8e, f), which is captured by existing characters codifying the degree of the proximal expansion (see the rotation of these areas respective to the distal end in Mannion et al. 2013: Ch231; also see the morphology of the proximal end in Mannion et al. 2013: Ch45 and Ch46 [considering the modification proposed by Upchurch et al. 2015]; and Upchurch et al. 2015: Ch283). This variability primarily reflects contrast of the robust and mediolaterally-expanded proximal end of the radii of Saltasauridae, versus the more mediolaterally-compressed radii of Colossosauria and some lithostrotians such as *Aeolosaurus* sp. (specimen MPCA-Pv-27174; Figs. 4e, f, 6c). There are also significant morphological differences along LD1 regarding the form of the medial face of the distal end of the radius. Specifically, these variations occur in the relative expansion and overall projection of the distal end, as

well as the angle produced by the bevelling of the medial corner of the distal end. These variations are already captured by phylogenetic characters concerning the expansion and bevelling of the distal end (bevelling of the distal end in Tschopp et al. 2015: Ch393 after Curry Rogers and Foster 2001; radius distal expansion in Tschopp et al. 2015: Ch394 after Wilson 2002). A character summarizing the orientation of the distal articulation also incorporates some of this variation (Wilson 2002: Ch171). LD2 in our analyses also captured some minor variability associated with the form of the distal end, which was linked with the forms of the medial and lateral margins of the distal shaft (Fig. 7f; both margins visible in anterior and posterior views). This variability is captured by a recently-proposed character regarding the relative bevelling of the distal end (Mannion et al. 2013: Ch49), and we note that some lithostrotians analysed here exhibit a lesser degree of torsion and only in the distal region of the shaft in comparison with other titanosaurs. Both morphotypes at Lo Hueco and *Elaltitan lilloi* exhibit a radius with slightly laterally-bevelled distal end whereas there is no torsion of the shaft (e.g. Morphotype I of Lo Hueco specimen HUE-1140 and *E. lilloi* PVL-4628). Meanwhile, other colossosaurs and saltasaurids present a completely bevelled distal end plus a curved axis of the shaft (e.g. *Mendozasaurus neguyelap* IANIGLA-70-1 and *Saltasaurus loricatus* specimen PVL.4017-77).

We also observed variation along LD1 in the central portion of the radius posterior surface (Fig. 8e). This variation reflects differences in the structure of the interosseous ridge, which captured by the phylogenetic character regarding the relative development of this ridge (Curry Rogers 2005: Ch283). It is also important to consider the medial portion of this region, dorsal to the posteromedial distal condyle. The posteromedial distal condyle exhibits an acute accessory ridge in some sauropod specimens (e.g. Morphotype II at Lo Hueco, HUE-1340), and it was found in our analyses to be related to differences in the more variable areas both along LD1 and LD2 (Fig. 7e, f). LD2 highlights differences between early-branching lithostrotians and representatives of Colossosauria and Saltasauridae (Fig. 4e), which exhibit, among other features, an absence of this acute accessory ridge (e.g. *Mendozasaurus neguyelap* specimen IANIGLA-PV-70-1). Some authors have reported an homologous ridge (e.g. posteromedial scar of *Rapetosaurus krausei*, Curry Rogers 2009) and it could be related to the attachment of *M. transversus palmaris* (e.g. *Saturnalia tupiniquim* Langer et al. 2007; however, the reconstruction is equivocal in *Dreadnoughtus schrani*, Voegele et al. 2020); but further data is needed in titanosaurians. Therefore, this variability could be incorporated into a potential new character regarding the development of an accessory and acute ridge dorsal to the posteromedial distal condyle, which is parallel to the interosseous ridge.

Lastly for the radius, there is also variation along LD2 in the posterior face just distal to the proximal end, which appears to reflect variable presence of a deep concavity in this area, which is observed in many of the sampled lithostrotian radii (e.g. Morphotype I at Lo Hueco, HUE-1140, HUE-2711; *Elaltitan lilloi* PVL-4628). In contrast, neither saltasaurids nor colossosaurs exhibit this concavity, regardless of the morphology of the proximal end (e.g. the anteriorly rotated triangle shaped proximal end in *Neuquensaurus australis*, specimen MLP-CS-1176; a more oval-shaped proximal end of *Saltasaurus loricatus*, specimen PVL-4017-78; or the extremely-compressed proximal end in *Muyelensaurus pecheni*, specimenMAU-PV-77). Further inspection of the morphology of the proximal end, as well as the proximal portion of the interosseous ridge among sauropods, could help to assess the potential quantification of these differences into a new phylogenetic character..

The femur exhibits quite subtle variations along each LD (Fig. 8a, b), probably caused by common morphological convergence as discussed above (see also Fig. 5a, b, 6d). Most of the variation along LD1 occurred in the proximalmost portion of the femoral head (Fig. 8a), which has been captured by a character describing the relative proximodistal displacement of the proximal end (see Royo-Torres 2009: Ch157; Gorscak et al. 2017: Ch241). This variability also involves the presence of a bulbous head separated from the rest of the proximal end by a sulcus between the femoral head and femoral trochanter, which has also been proposed as two separate phylogenetic characters (Royo-Torres 2009: Ch158 and the following unnumbered character, p.321).

Other areas of the femur exhibiting noteworthy variation along LD1 include the lateral bulge, especially its anterodistal portion (Fig. 8a). Differences were found in the anteroposterior width of the lateral bulge between saltasaurids and other somphospondylans, and this has not previously been used as a phylogenetic character. The closest character to date that has come to reflect this variability, is a character that only notes the presence of the lateral bulge (e.g. Calvo and Salgado 1995: Ch47; Salgado et al. 1995 1997: Ch19; Wilson 2002; Ch199). Use of a new character focused on the anteroposterior width of the lateral bulge could be helpful to incorporate these morphological differences among distinct sauropod clades (Fig. 6a). Another important, related observation is the presence of an anterior deflection of the lateral bulge, as seen in some Ibero-Armorican lithostrotians (Vila et al. 2012; Páramo et al. 2016). This feature has not been considered in any cladistic analysis to date, but further assessment in other titanosaurian taxa could be helpful, as it has been found to vary among different titanosaurian clades in our analyses (Fig. 8a).

Finally, the analysed femora exhibit considerable variation in the forms of the distal condyles: specifically, the tibial condyle along LD1, and the fibular condyle along LD2 (Fig. 8a, b). Differences in the tibial condyle are concentrated in the posterior face of the femur (Fig. 8a) and appear related to minor differences in the shape of the fibular condyle; these variations primarily differentiate saltasaurids from other somphospondylans (Fig. 5c). The mediolateral width ratio between the fibular and tibial condyles has been examined previously, and our analyses are congruent with prior character scoring differences (see Wilson 2002: Ch200). However, our results also highlight the posterior projection of the distal condyles and the relative expansion of the tibial condyle as the primary aspect of variation. More recent studies have proposed a character based on these observed differences via qualitative anatomical comparison (Whitlock 2011: Ch179; Poropat et al. 2016: Ch389; Mannion et al. 2019: Ch535) but lack the anteroposterior expansion of the distal condyles. However, considering comments by Royo-Torres (2009: see his comments on anteroposterior projection of the condyles in Ch171) and our results, it would be beneficial to adjust the definition of this character. In addition, variability in the shape of the fibular condyle (along LD2, Fig. 8b) reflects differences observed in the orientation of the lateral epicondyle on the posterior-posterolateral surface of the fibular condyle. Our analyses suggest it may be useful to define a new character related to the relative orientation of this feature on the lateral margin of the fibular condyle.

The tibiae exhibit distinct variation across LD1 at the lateral and medial margin of the proximal end (Fig. 8). These differences occur between the more compressed, triangular shaped proximal end typical of titanosaurs (e.g. *Lohuecotitan pandafilandi,* HUE-3082), the more expanded but rounded proximal end of saltasaurids (e.g. *Neuquensaurus*, MLP-CS-1093) and the oval-shaped and extremely mediolaterally compressed proximal end of colossosaurs (e.g. *Muyelensaurus pecheni*, MAU-PV-162). Some lithostrotians exhibit a mediolaterally-compressed proximal end, like the tibia MCNA-13860, referred to *Lirainosaurus astibiae*; which is found in the non-saltasaurid lithostrotian region of the LDA morphospace, not pooled with other colossosaurian specimens. The tibia of *L. astibiae* is plotted close to the specimens of early-branching titanosaurs, indicative that it still exhibits a plesiomorphic morphology (Figs. 5c, 6e: see the mediolaterally compressed tibia of *L. astibiae* that is plotted closer to *Antarctosaurus wichmannianus* specimen MACN-6804-22 in the LDA). These variations are already captured by established characters regarding the morphology of the proximal end of the tibia (Wilson 2002: Ch203; Royo-Torres 2009: Ch172) and the development of the fibular articulation (see discussion on Ch291 in Harris 2006; Royo-Torres 2009: Ch179; Tschopp et al. 2015: Ch445; Mannion et al. 2017: Ch416). However, two additional distinctive morphologies can be observed in our analyses in this portion of the tibia. The first is related to the presence of a secondary cnemial crest as in other somphospondylii (e.g. *Janenschia robusta* Bonaparte et al. 2000; Mannion et al. 2013, 2019; *Dreadnoughtus schrani*, *Gobititan shenzhouensis*, *Antarctisaurus wichmannianus*, *Uberabatitan riberoi* and weakly present in *Atsinganosaurus velauciensis*, Ullmann and Lacovara 2016) and probably in *Lohuecotitan pandafilandi*, as well as some specimens of Morphotype I at Lo Hueco (Díez Díaz et al. 2016; Páramo et al. 2017a, b). A recent study noted the presence of this feature in several sauropods (Mannion et al. 2013: Ch261). The second feature is the presence of a more complex articulation with the fibula in the posterior portion of the proximal end. Our analyses indicate variability in this region due to differences between both saltasaurids and other titanosaurs along LD1 and colossosaurs and other titanosaurs along LD2 (Figs. 6e, 8c, d). The differences relate to the development of a concavity and an accessory ridge in the posterolateral region of the proximal end in some titanosaurs, as in Morphotype II at Lo Hueco (e.g. HUE-1149 and HUE-4055) and *Mendozasaurus neguyelap* (e.g. IANIGLA-74-1). This accessory fibular articular ridge is also found in some mamenchisaurids (Young and Zhao 1972; Royo-Torres 2009). Thus, a new character regarding this protrusion or accessory ridge on the posterior face of the proximal end could be developed to capture this morphological variability observed by other authors (Royo-Torres 2009: Ch180) and in our analyses. Finally, the variability in the medial face of the tibia appears to be related to the degree of curvature of the proximal end as seen in proximal view, as discussed above. An existing phylogenetic character regarding the morphology of the proximal end of the tibia (Wilson 2002: Ch203) already incorporates these variations.

We also found great variation in the distal end, specifically in the form of the articular surface for the ascending process and the medial face of the distal end (Fig. 8c, d). Variability along the medial surface as well as the anterior and posterior margins of the distal end, are largely captured by characters describing the distal expansion of the tibia (Wilson 2002: Ch205; Royo-Torres 2009: Ch184) and the relative proportions of the anteroposterior width to the mediolateral width of the distal end (Salgado et al. 1997: Ch7; Royo-Torres 2009: Ch183 and Ch184; Mannion et al. 2013: Ch68). These variations are also related to the relative position of the articular surface for the ascending process and the rotation of the distal end respective to the axis of the shaft (Figs. 5c, d, 6e, 8c, d). The rotation of the distal condyle of the tibia was originally described by Sanz et al. (1999: Ch42) and if used in additional future phylogenetic studies would incorporate the variations observable in our morphometric analyses. However, another osteological character is

necessary to incorporate the variation in the orientation of distal condyle respective to the orientation of the cnemial crest, as also suggested by our morphometric analyses.

The distal portion of the cnemial crest also exhibits considerable variability along LD2 (Fig. 8d). The proximodistal morphology of the cnemial crest has recently been used as a phylogenetic character (Tschopp et al. 2015: Ch444), but the formulation of that character is too vague to capture the variability among most of the analysed somphospondylans, saltasaurids, colossosaurs and *Aeolosaurus* sp specimen MPCA-Pv-27100-8, as found in our analyses (Figs. 5c, 6e). Early branching titanosaurians commonly exhibit a rounded morphology in lateral view (e.g. *Bonatitan reigi* specimen MACN-PV-RN-821, *Lohuecotitan pandafilandi* HUE-3082), whereas saltasaurids exhibit a triangle-shaped cnemial crest (e.g. *Saltasaurus loricatus*, PVL-4017-46), or sometimes a combination of rounded proximal with straighter distal portion of the cnemial crest (e.g. "*Neuquensaurus robustus*" specimen MCS-6) which is also shared with some colossosaurs (*Mendozasaurus neguyelap*, IANIGLA-74-1) and some lithostrotians (*Atsinganosaurus velauciensis* specimen MMS/VBN-02.90, Díez Díaz et al. 2018a, b). For this reason, we believe it would be beneficial to implement additional characters or additional states to that character describing the morphology of the cnemial crest in lateral view in future cladistic analyses, such as in Royo-Torres (2009: Ch177).

Lastly, the fibulae exhibit variation along LD1 in their posterior profiles, especially in the region distal to the lateral trochanter (Fig. 8e). These variations involve development of a sigmoid fibular shaft, easily visible in lateral view, due primarily to the curvature of the distal shaft relative to the proximal end. This variability is already incorporated in characters describing the sigmoid profile of the fibula (e.g. D'Emic 2012: Ch113). There are variations in the anterior portion of the proximal end, particularly differences in the shape of the anterior trochanter that collectively alter the shape of the proximal end (D'Emic 2012: Ch111 and Ch112), as well as in the development and anterior versus medial projection of the anterior trochanter (Royo-Torres 2009: Ch189 and the following unnumbered character p.369; D'Emic 2012: Ch111; Tschopp et al. 2015: Ch447). Our analyses also support inclusion of the phylogenetic characters proposed by Royo-Torres (2009: unnumbered character based on Borsuk-Bialynicka 1977, p.371) regarding the morphology of the proximal end and anterior trochanter, as some of the variability along LD2 is also concentrated in the posterolateral corner of the proximal end (Fig. 8f).

We also observed variability along LD1 in the shape of the anterior portion of the distal end of the fibula, specifically both the anterolateral crest and the anterior face of the distal end (Fig. 8e). These variations have been recently incorporated as new characters regarding the morphology of the distal end and its profile (Poropat et al. 2016: Ch394; Mannion et al. 2019: Ch394). However, it would likely be beneficial to further explore the development and the mediolateral torsion of the distal anterolateral crest (Fig. 8e) as a new character(s), which could potentially cover the more subtle morphological differences observed in our analyses.

4.3 Caveats of this study

Our analysis includes a wide sample of sauropod elements comprising parts of the non-autopodial limb skeleton of titanosaurs. However, the sample included here comprises taxa with almost all element types represented (e.g. *Neuquensaurus* spp. *Muyelensaurus pecheni*, etc.); more incomplete taxa preserving only some of these appendicular elements are still excluded even though they may exhibit relevant data (e.g. the humerus of *Nothocolossus gonzalezparejasi* and the fibula of *Argentinosaurus huinculensis* could add meaningful data for comparison). In order to propose new morphological characters, additional specimens should be surveyed, although we opted to provide a preliminary discussion for potential new character definitions or alternative codifications for phylogenetic characters already in common use. We chose a conservative approach given the bias towards better-preserved titanosaurs (both most complete specimens and least taphonomically-altered specimens), especially from lithostrotian subclades, in this study.

Despite the abundant sample of titanosaurian remains from Lo Hueco with several well-to-decently preserved elements, the fossils make it difficult both to digitize of complete meshes due to the fragmentary or distorted state of the specimen and to sample complete suites of landmarks. The most common issue is lack of preservation of some portions of the bone that results in missing landmarks or semilandmark curves along lost structures of specimens (commonly the proximal and distal ends of titanosaurian long bones, e.g. Morphotype I at Lo Hueco, tibia HUE-2669). Sometimes an incomplete mesh representation of an actual specimen can still be used to determine the probable placement of landmark and semilandmark curves (e.g. *Saltasaurus loricatus*, ulna PVL-4017-72). In these cases, the landmark and semilandmark curves can still be analysed, but the mesh of the specimen cannot be used for projection and sliding of the surface semilandmarks. Therefore, we used estimation techniques for the actual landmark coordinates, and then produce a new and complete mesh that can act as a proxy of the specimen true mesh. Traditionally in the absence of landmarks, researchers exclude those landmarks or incomplete specimens, but the exclusion of potential informative areas or taxa can hinder palaeobiological studies (Brown et al. 2012) and estimation of landmarks can therefore be a more comprehensive and informative procedure (Brown et al. 2012; Arbour and Brown 2014).

In order to control for potential errors caused by the estimation of landmark coordinates and the resulting meshes obtained by statistical-virtual restoration, we tested the effects of our estimations. Specifically, we produced a bootstrap sample of specimens to assess differences via intra-landmark Procrustes distances between the different sets of estimated landmarks of the bootstrap sample. We also compared the meshes obtained from virtual restoration with the function *vcgMetro*(), which applies the command line "*metro*" (Cignoni et al. 1998), included in the *Rvcg* v.0.18 package (Schlager 2017). No specimen of the estimated dataset exhibits significantly high deviation in the landmark positions and the variance from each bootstrap sample fell below the differences observed in this study (< 1 mm). The deviation in the virtually restored meshes falls below ~ 3 mm error for all the analysed elements, which is still less than that of some digitizing methods (e.g. IR-scanning following Falkingham 2012). Therefore, data estimation error does not bias our results.

5 Conclusions

The sauropod appendicular skeleton exhibits morphological similarities between phylogenetically-distinct clades. The most probable driving force behind morphospace convergences is that these features reflect ecomorphological similarities rather than phylogenetic affinities. Distinct clades can acquire a similar morphology based on different morphofunctional traits. Saltasaurids are the only clade clearly different from other somphospondylans analysed here (e.g. they plot isolated in the PCA and LDA for most of the analysed limb elements). Among the analysed titanosaurs, we found that Morphotype II at Lo Hueco occupies a similar morphospace to colossosaurs like *Mendozasaurus neguyelap* and *Muyelensaurus pecheni*. This means that Morphotype II at Lo Hueco exhibits a similar morphofunctional specialization to those mid-sized colossosaurians. The ulnae and tibiae of Morphotype II at Lo Hueco exhibit similarities to the morphology of those of *Mendozasaurus neguyelap* and our PCAs plot them in the same region of the morphospace, separated from other lithostrotian specimens. The similarities in morphospace occupation may not have a phylogenetic meaning. However, when the morphospaces are calculated by maximizing the between group differences with LDA, Morphotype II specimens were placed within the same region of the morphospace as other lithostrotians. In contrast, Morphotype I at Lo Hueco exhibit morphological similarities to other titanosaurian taxa like *Jainosaurus* cf. *septentrionalis* in all the analysed elements and usually overlaps the morphospace region of more early-branching titanosaurians in our PCA and LDA. Generally, the analysed somphospondylans (excluding Colossosauria and saltasaurid lithostrotians) share a similar morphospace.

Saltasauridae are the only exception to the general pattern of overlapping found in our PCAs between different titanosaurian clades, as they are found to occupy a unique morphospace in both our PCA and LDA, indicating that they present an entire unique morphofunctional morphospace occupation. The distinctly robust and arched limb morphology previously regarded as representative of "wide-gauge" titanosaurian posture may be instead a relatively derived variant of this stance, while all the other sampled titanosaurs exhibit the apomorphic features related to a less extreme "wide-gauge" stance. It is also important to take into account that previous studies highlighted the sampling bias towards well-known titanosaurs that are representatives of Saltasauridae (e.g. *Opisthocoelicaudia skarzinskii*, *Alamosaurus sanjuanensis*, *Neuquensaurus* spp. and *Saltasaurus loricatus*). Our results may add another potential issue to these claims, as the low sample size of other titanosaurs outside Saltasauridae may further bias the analyses and anatomical comparisons towards a derived and specialized appendicular morphology. Members of Saltasauridae exhibit a clearly different appendicular morphology in comparison with other non-saltasaurid titanosaurs (also noticed by Carrano 2006; González Riga et al. 2019). Our results are congruent with the proposal of González Riga et al. (2019) to further increase the sample of more non-saltasaurid titanosaurs in the analyses.

In this study, we found the separation of Colossosauria in a GMM analysis for the first time, and looked for any potential new phylogenetically-relevant characters observable after the inclusion of this clade of non-lithostrotian sauropods (as well as other 'intermediate' titanosaurs). Overall, our results are congruent with current phylogenetic information (particularly Gonzalez Riga et al. 2018, 2019; Mannion et al. 2019). Moreover, our analyses allowed the proposal of several new characters regarding bone regions previously not represented in morphological datasets used in cladistic analyses. Our analyses also support the future inclusion of some morphological characters not considered in current phylogenetic data matrices (e.g. anterior projection of lateral bulge, Vila et al. 2012; the secondary posterolateral ridge of the fibular articulation of the tibia, Royo Torres 2009) as they appear more widespread among titanosaurian subclades. GMM has proved to be a useful tool to assess morphological variability in the appendicular skeleton and to identify the most variable areas in it despite its conservative morphology and overlapping between exclusive clades. We have shown that it is possible to identify the bone regions which exhibit most of the morphological variation that may reflect differences between titanosaurian clades.

Acknowledgements This research was funded by project CGL2012-35199 and CGL2015-68363-P from the Ministry of Economy and Competitiveness of Spain. Research of A. Páramo was funded by contract BES-2013-065509 granted by the Ministry of Economy and Competitiveness of Spain. Preparation and study of material from Lo Hueco was possible under projects SBPLY/15/180601/000045, SBPLY/16/180801/000017, SBPLY/17/ 180801/000063 of the Junta de Comunidades de Castilla-La Mancha, Spain. We want to thank also F. Marco-Fernández and the Conservacion GBE team as well as the alumni of Methodology of Archaeological Materials, Conservation and Restoration of Cultural Heritage degree (Fine Arts Faculty, UCM, Spain) and the alumni from the Taller de Restauración Paleontológica I, II & III, Cuenca (C-LM, Spain). Access to Argentinean titanosaurian material was possible thanks to the funding EEBB-I-16-11875 from the Ministry of Economy and Competitiveness of Spain. Access to NHM collections was possible thanks to funding of European Union SYNTHESYS program 2016. Ref. GB-TAF-6153. Research of P. Mocho was funded by FCT/MCTES for one CEEC Individual contract (CEECIND/00726/2017). We want to also thank the following people for access to the sampled specimens under their care to S. Langreo from the Museo de Paleontología de Castilla-La Mancha (Cuenca, Spain); J.A. Ramírez de la Peciña and C. Corral from the MCNA (Vitoria, Spain); R. Coria from the MCF (Plaza Huincul, Argentina); L. Filippi from the MRS (Rincón de los Sauces, Argentina); M. Reguero from the MLP (La Plata, Argentina) and A. Otero from the CONICET (La Plata, Argentina); S. Devincenzi from the IANIGLA (Mendoza, Argentina) and B. González Riga from the UNCUYO (Mendoza, Argentina); C. Muñoz from the MPCA (Cipolletti, Argentina) and I. Cerda from the CONICET (Cipolletti, Argentina); P. Ortiz from the PVL (Tucumán, Argentina); A.G. Kramarz and M. Ezcurra from the MACN (Buenos Aires, Argentina). We want to also thank P. Ullmann and an anonymous reviewer for their commentaries and suggestions that allowed to improve this article.

Author contributions PA: conceptualization, formal analysis, investigation, methodology, resources, writing—original draft, writing—review and editing. MP: investigation, resources, writing—review and editing. OF: conceptualization, funding acquisition, investigation, project administration, supervision, writing—review and editing.

Funding This research was funded by project CGL2012-35199 and CGL2015-68363-P from the Ministry of Economy and Competitiveness of Spain. Work from Páramo, A. was funded by contract BES-2013-065509 granted by the Ministry of Economy and Competitiveness of Spain. Preparation and study of Material from Lo Hueco was possible under projects SBPLY/15/180601/000045, SBPLY/16/180801/000017, SBPLY/17/ 180801/000063 of the Junta de Comunidades de Castilla-La Mancha, C-LM, Spain. Access to Argentinean titanosaurian material was possible thanks to the funding EEBB-I-16-11875 from the Ministry of Economy and Competitiveness of Spain. Access to NHM collections was possible thanks to the funding European Union SYNTHESYS program 2016. Ref. GB-TAF-6153. Work by Mocho, P. was funded by FCT/MCTES through one CEEC Individual contract (CEECIND/00726/2017).

Data availability Online Resources (various, cited in manuscript text).

Code availability R-code available in Online Resource 6.

Compliance with ethical standards

Conflict of interest The authors declare that they have no conflict of interest.

References

Adams, D. C., Collyer, M. L., & Kaliontzopoulou, A. (2019). Geomorph: Software for geometric morphometric analyses. R package version 3.1.0. https://cran.r-project.org/package=geomorph.

Adler, D., Murdoch, D., et al. (2019). rgl: 3D visualization using OpenGL. https://cran.r-project.org/package=rgl.

Apesteguía, S. (2005). Evolution of the titanosaur metacarpus. In V. Tidwell & K. Carpenter (Eds.), *Thunder-lizards: The sauropodomorph dinosaurs* (pp. 321–345). Bloomington: Indiana University Press.

Arbour, J. H., & Brown, C. M. (2014). Incomplete specimens in geometric morphometric analyses. *Methods in Ecology and Evolution, 5*(1), 16–26.

Bates, K. T., Mannion, P. D., Falkingham, P. L., Brusatte, S. L., Hutchinson, J. R., Otero, A., et al. (2016). Temporal and phylogenetic evolution of the sauropod dinosaur body plan. *Royal Society Open Science*. https://doi.org/10.1098/rsos.150636.

Blender Online Community (2018). Blender - a 3D modelling and rendering package. Blender Institute, Amsterdam. URL http://www.blender.org

Bonaparte, J. F., Heinrich, W.-D., & Wild, R. (2000). Review of *Janenschia* WILD, with the description of a new sauropod from the Tendaguru beds of Tanzania and a discussion on the systematic value of procoelous caudal vertebrae in the sauropoda. *Palaeontographica Abteilung A, 256*(1–3), 25–76.

Bonnan, M. F. (2004). Morphometric analysis of humerus and femur shape in Morrison sauropods: Implications for functional morphology and paleobiology. *Paleobiology, 30*(3), 444–470.

Bonnan, M. F. (2007). Linear and geometric morphometric analysis of long bone scaling patterns in Jurassic neosauropod dinosaurs: Their functional and paleobiological implications. *Anatomical Record, 290*(9), 1089–1111.

Bookstein, F. L. (1991). *Morphometric tools for landmark data*. Cambridge: Cambridge University Press.

Borsuk-Bialynicka, M. (1977). A New Camarasaurid Sauropod *Opisthocoelicaudia skarzynskii* gen. n., sp. n. from the Upper Cretaceous of Mongolia. *Paleontologia Polonica, 37*, 5–64.

Botton-Divet, L., Houssaye, A., Herrel, A., Fabre, A.-C., & Cornette, R. (2015). Tools for quantitative form description; an evaluation of different software packages for semi-landmark analysis. *PeerJ, 3*, e1417.

Brown, C. M., Arbour, J. H., & Jackson, D. A. (2012). Testing of the effect of missing data estimation and distribution in morphometric multivariate data analyses. *Systematic Biology, 61*(6), 941–954.

Canudo, J. I. (2001). Descripción de un fragmento proximal de fémur de Titanosauridae (Dinosauria, Sauropoda) del Maastrichtiense superior de Serraduy (Huesca). In G. Meléndez, Z. Herrera, G. Delvene, & B. Azanza (Eds.), *XVII Jornadas de Paleontología. Los fósiles y la Paleogeografía* (pp. 255–262). Zaragoza: Sociedad Española de Paleontología y Áreay Museo de Paleontología de la Universidad de Zaragoza.

Carballido, J. L., Marpmann, J. S., Schwarz, D., & Pabst, B. (2012). New information on a juvenile sauropod specimen from the Morrison Formation and the reassessment of its systematic position. *Palaeontology*. https://doi.org/10.1111/j.1475-4983.2012.01139.x.

Carballido, J. L., Pol, D., Cerda, I. A., & Salgado, J. L. (2011). The Osteology of *Chubutisaurus insignis* Del Corro, 1975 (Dinosauria: Neosauropoda) from the "Middle" Cretaceous of Central Patagonia, Argentina. *Journal of Vertebrate Paleontology, 31*(1), 93–110.

Carballido, J. L., Pol, D., Otero, A., Cerda, I. A., Salgado, J. L., Garrido, A. C., et al. (2017). A new giant titanosaur sheds light on

body mass evolution among sauropod dinosaurs. *Proceedings of the Royal Society B Biological Sciences*. https://doi.org/10.1098/rspb.2017.1219.

Carballido, J. L., & Sander, P. M. (2014). Postcranial axial skeleton of *Europasaurus holgeri* (Dinosauria, Sauropoda) from the Upper Jurassic of Germany: Implications for sauropod ontogeny and phylogenetic relationships of basal Macronaria. *Journal of Systematic Palaeontology, 12*(3), 335–387.

Carrano, M. T. (1998). Locomotion in non-avian dinosaurs: Integrating data from hindlimb kinematics, in vivo strains, and bone morphology. *Paleobiology, 24*(4), 450–469.

Carrano, M. T. (2005). The evolution of sauropod locomotion. In K. A. CurryRogers & J. A. Wilson (Eds.), *The Sauropods: Evolution and paleobiology* (pp. 229–250). California: University of California Press.

Carrano, M. T. (2006). Body-size evolution in the Dinosauria. In M. T. Carrano, T. J. Gaudin, R. W. Blob, & J. Wible (Eds.), *Amniote paleobiology: Perspectives on the evolution of mammals, birds, and reptiles* (pp. 225–268). Chicago: University of Chicago Press.

Christian, A., & Dzemski, G. (2011). Neck posture in Sauropods. In *Biology of the Sauropod Dinosaurs: Understanding the life of giants* (pp. 251–262).

Cignoni, P., Rocchini, C., & Scopigno, R. (1998). Metro: Measuring error on simplified surfaces. *Computer Graphics Forum, 17*(2), 167–174.

Claude, J. (2008). *Morphometrics with R. Use R!*. New York: Springer.

Company, J., Suberbiola, X. P., & Ruiz-Omeñaca, J. I. (2009). Nuevos restos fósiles del dinosaurio *Lirainosaurus*. *Ameghiniana, 46*(2), 391–405.

Curry Rogers, K. (2005). Titanosauria: A phylogenetic overview. In K. Curry Rogers & J. A. Wilson (Eds.), *The Sauropods: Evolution and paleobiology* (pp. 50–103). Berkeley: University of California Press.

Curry Rogers, K. (2009). The postcranial osteology of *Rapetosaurus krausei* (Sauropoda: Titanosauria) from the Late Cretaceous of Madagascar. *Journal of Vertebrate Paleontology*, *29*(4), 1046–1086.

D'Emic, M. D. (2012). The early evolution of titanosauriform sauropod dinosaurs. *Zoological Journal of the Linnean Society, 166*, 624–671.

D'Emic, M. D., Mannion, P. D., Upchurch, P., Benson, R. B. J., Pang, Q., & Zhengwu, C. (2013). Osteology of *Huabeisaurus allocotus* (Sauropoda: Titanosauriformes) from the Upper Cretaceous of China. *PLoS One*. https://doi.org/10.1371/journal.pone.0069375.

Darlington, R. B., Weinberg, S. L., & Walberg, H. J. (1973). Canonical variate analysis and related techniques. *Review of Educational Research, 43*, 433–454.

Díez Díaz, V., Garcia, G., Pereda Suberbiola, X., Jentgen-Ceschino, B., Stein, K. H. W., Godefroit, P., & Valentin, X. (2018). A new titanosaurian sauropod from the Late Cretaceous of Velaux-La Bastide Neuve (southern France). In *XVI annual meeting of the European association of vertebrate paleontologists* (p. 60). Caparica, Lisbon.

Díez Díaz, V., Garcia, G., Pereda-Suberbiola, X., Jentgen-Ceschino, B., Stein, K., Godefroit, P., et al. (2018). The titanosaurian dinosaur *Atsinganosaurus velauciensis* (Sauropoda) from the Upper Cretaceous of southern France: New material, phylogenetic affinities, and palaeobiogeographical implications. *Cretaceous Research, 91*, 429–456.

Díez Díaz, V., Mocho, P., Páramo, A., Escaso, F., Marcos-Fernández, F., Sanz, J. L., et al. (2016). A new titanosaur (Dinosauria, Sauropoda) from the Upper Cretaceous of Lo Hueco (Cuenca, Spain). *Cretaceous Research, 68*, 49–60.

Díez Díaz, V., Pereda Suberbiola, X., & Company, J. (2015). Updating titanosaurian diversity (Sauropoda) from the Late Cretaceous of Spain: The fossil site of Laño and Chera. *Spanish Journal of Palaeontology, 30*(2), 293–306.

Díez Díaz, V., Suberbiola, X. P., & Sanz, J. L. (2013). Appendicular skeleton and dermal armour of the Late Cretaceous titanosaur *Lirainosaurus astibiae* (Dinosauria: Sauropoda) from Spain. *Palaeontologia Electronica, 16*(2), 18p.

Falkingham, P. L. (2012). Acquisition of high resolution three-dimensional models using free, open-source, photogrammetric software. *Paleontologia Electronica, 15*(1), 1–15.

Falkingham, P. L. (2013). Low cost 3D scanning using off-the-shelf video gaming peripherals. *Journal of Paleontological Techniques, 11*, 1–9.

Garcia, G., Amico, S., Fournier, F., Thouand, E., & Valentin, X. (2010). A new Titanosaur genus (Dinosauria, Sauropoda) from the Late Cretaceous of southern France and its paleobiogeographic implications. *Bulletin de la Société Géologique de France*, *181*(3), 269–277.

González Riga, B. J. (2003). A new Titanosaur (Dinosauria, Sauropoda) from the Upper Cretaceous of Mendoza Province, Argentina. *Ameghiniana, 40*(2), 155–172.

González Riga, B. J., Lamanna, M. C., Ortiz David, L. D., Calvo, J. O., & Coria, J. P. (2016). A gigantic new dinosaur from Argentina and the evolution of the sauropod hind foot. *Scientific Reports, 6*(1), 1–15.

González Riga, B. J., Lamanna, M. C., Otero, A., Ortiz David, L. D., Kellner, A. W. A., & Ibiricu, L. M. (2019). An overview of the appendicular skeletal anatomy of South American titanosaurian sauropods, with definition of a newly recognized clade. *Anais Da Academia Brasileira de Ciências*. https://doi.org/10.1590/0001-3765201920180374.

González Riga, B. J., Mannion, P. D., Poropat, S. F., Ortiz David, L. D., & Coria, J. P. (2018). Osteology of the Late Cretaceous Argentinean sauropod dinosaur *Mendozasaurus neguyelap*: Implications for basal titanosaur relationships. *Zoological Journal of the Linnean Society, 20*, 1–46.

Gorscak, E., & O'Connor, P. M. (2016). Time-calibrated models support congruency between Cretaceous continental rifting and titanosaurian evolutionary history. *Biology Letters, 12*(4), 20151047.

Gorscak, E., O'Connor, P. M., Roberts, E. M., & Stevens, N. J. (2017). The second titanosaurian (Dinosauria: Sauropoda) from the middle Cretaceous Galula Formation, southwestern Tanzania, with remarks on African titanosaurian diversity. *Journal of Vertebrate Paleontology, 37*(4), e1343250.

Gunz, P. (2005). *Statistical and geometric morphometric reconstruction of hominid crania. Reconstructing autralopithecine ontogeny*. Vienna: University of Vienna.

Gunz, P., & Mitteroecker, P. (2013). Semilandmarks: A method for quantifying curves and surfaces. *Hystrix The Italian Journal of Mammalogy, 24*(1), 103–109.

Gunz, P., Mitteroecker, P., & Bookstein, F. L. (2005). Semilandmarks in three dimensions. In D. E. Slice (Ed.) *Modern morphometrics in physical anthropology* (pp. 73–98).

Gunz, P., Mitteroecker, P., Neubauer, S., Weber, G. W., & Bookstein, F. L. (2009). Principles for the virtual reconstruction of hominin crania. *Journal of Human Evolution, 57*(1), 48–62.

Harris, J. D. (2006). The significance of *Suuwassea emilieae* (Dinosauria: Sauropoda) for flagellicaudatan intrarelationships and evolution. *Journal of Systematic Palaeontology, 4*(2), 185–198.

Henderson, D. M. (2006). Burly gaits: Centers of mass, stability, and the trackways of sauropod dinosaurs. *Journal of Vertebrate Paleontology, 26*(4), 907–921.

Jakob, W., Tarini, M., Panozzo, D., & Sorkine-Hornung, O. (2015). Instant field-aligned meshes. In *ACM transactions on graphics (proceedings of SIGGRAPH Asia 2015)* (pp. 1–15).

Kendall, D. G. (1984). Shape manifolds, procrustean metrics, and complex projective spaces. *Bulletin of the London Mathematical Society, 16*(2), 81–121.

Langer, M. C., Franca, M., & Gabriel, S. (2007). The pectoral girdle and forelimb anatomy of the stem-sauropodomorph *Saturnalia tupiniquim* (Upper Triassic, Brazil). *Special Papers in Palaeontology, 77*, 113–137.

Lautenschlager, S. (2017). From bone to pixel—fossil restoration and reconstruction with digital techniques. *Geology Today, 33*(4), 155–159.

Lautenschlager, S., Rayfield, E. J., Altangerel, P., Zanno, L. E., & Witmer, L. M. (2012). The endocranial anatomy of therizinosauria and its implications for sensory and cognitive function. *PLoS One, 7*(12), e52289.

Le Loeuff, J. (1995). *Ampelosaurus atacis* (nov, gen., nov. sp.), un nouveau Titanosauridae (Dinosauria, Sauropoda) du Crétacé supérieur de la Haute Vallée de l'Aude (France). *Comptes Rendus de l'Académie Des Sciences à Paris Série IIa, 321*, 693–699.

Le Loeuff, J. (2005). Osteology of Ampelosaurus atacis (Titanosauria) from Southern France. In V. Tidwell & K. Carpenter (Eds.), *Thunder-lizards: The sauropodomorph dinosaurs* (1st ed., pp. 115–137). Bloomington: Indiana University Press.

Lydekker, R. (1893). The dinosaurs of patagonia. *Anales Del Museo de La Plata, 2*, 1–14.

Mallison, H., & Wings, O. (2014). Photogrammetry in paleontology—a practical guide. *Journal of Paleontological Techniques, 12*, 1–13.

Mannion, P. D., Allain, R., & Moine, O. (2017). The earliest known titanosauriform sauropod dinosaur and the evolution of Brachiosauridae. *PeerJ, 5*, e3217.

Mannion, P. D., Schwarz, D., Upchurch, P., & Wings, O. (2019). Taxonomic affinities and biogeographic implications of the putative titanosaurs (Dinosauria: Sauropoda) from the Late Jurassic Tendaguru Formation of Tanzania. *Journal of Vertebrate Paleontology, XX*, 1–126.

Mannion, P. D., Upchurch, P., Barnes, R. N., & Mateus, O. (2013). Osteology of the Late Jurassic Portuguese sauropod dinosaur *Lusotitan atalaiensis* (Macronaria) and the evolutionary history of basal titanosauriforms. *Zoological Journal of the Linnean Society, 168*(1), 98–206.

Mannion, P. D., Upchurch, P., Mateus, O., Barnes, R. N., & Jones, M. E. H. (2012). New information on the anatomy and systematic position of *Dinheirosaurus lourinhanensis* (Sauropoda: Diplodocoidea) from the Late Jurassic of Portugal, with a review of European diplodocoids. *Journal of Systematic Palaeontology, 10*, 1–31.

Mitteroecker, P., & Bookstein, F. L. (2011). Linear discrimination, ordination, and the visualization of selection gradients in modern morphometrics. *Evolutionary Biology, 38*(1), 100–114.

Mocho, P., Escaso, F., Marcos-Fernández, F., Páramo, A., Vidal, D. & Ortega, F. (2019b). Preliminary systematic overview on a new titanosaurian specimen from the Upper Cretaceous of Lo Hueco (Cuenca, Spain). In *17th annual meeting of the European Association of Vertebrate Palaeontology* (p. 76).

Mocho, P., Páramo, A., Díez Díaz, V., Escaso, F., Marcos-Fernández, F., Sanz, J.L. & Ortega & F. (2016). Looking through the axial skeleton of the Lo Hueco titanosaurians. In: Torcida Fernández-Baldor, F., Canudo, J.I., Huerta, P., Pereda, X. (Eds.), *VII International symposium about dinosaurs palaeontology and their environment* (pp. 99–100).

Mocho, P., Páramo, A., Escaso, F., Marcos-Fernández, F., Vidal, D. & Ortega, F. (2019c). Titanosaurians from Lo Hueco (Campanian–Maastrichtian) reveal new information about the evolutionary history of European titanosaurians. In *63rd annual meeting of the Paleontological Association* (pp. 110–111).

Mocho, P., Páramo, A., & Ortega, F. (2019a). Titanosaurians from the Iberian Peninsula: An overview and future perspectives. In *VIII international symposium about dinosaurs palaeontology and their environment*.

Mocho, P., Pérez-García, A., Martín-Jiménez, M., Ortega, F., Martín Jiménez, M., & Ortega, F. (2018). New remains from the Spanish Cenomanian shade light on the Gondwanan origin of European Early Cretaceous titanosaurs. *Cretacaceous Research*. https://doi.org/10.1016/j.toxlet.2014.06.131.

Molnar, J. L., Pierce, S. E., & Hutchinson, J. R. (2012). Idealized landmark-based geometric reconstructions of poorly preserved fossil material: A case study of an early tetrapod vertebra. *Palaeontologia Electronica, 15*(1), 1–18.

Ortega, F., Bardet, N., Barroso-Barcenilla, F., Callapez, P. M. P. M., Cambra-moo, O., Daviero- Gómez, V., et al. (2015). The biota of the Upper Cretaceous site of "Lo Hueco" (Cuenca, Spain). *Journal of Iberian Geology, 41*(1), 83–99.

Otero, A. (2010). The appendicular skeleton of *Neuquensaurus*, a Late Cretaceous saltasaurine sauropod from Patagonia, Argentina. *Acta Palaeontologica Polonica, 55*(3), 399–426.

Otero, A. (2018). Forelimb musculature and osteological correlates in Sauropodomorpha (Dinosauria, Saurischia). *PLoS One, 13*(7), e0198988.

Páramo, A., Mocho, P., Marcos-Fernández, F., Ortega, F., & Sanz, J. L. (2017). 3D geometric morphometrics on the hind limb of the Titanosaurs from Lo Hueco: Dwarf taxa or Small Individuals? In 15th annual meeting of the European Association of Vertebrate Paleontologists. *Zitteliana, 91*, 68.

Páramo, A., Mocho, P., Ortega, F., & Sanz, J. L. (2018). Intraspecific variability in and its effects on systematic assessment of the titanosaurs from Lo Hueco (Late Cretaceous. Cuenca, Spain). In *XVI annual meeting of European Association of Vertebrate Paleontologists* (p. 147).

Páramo, A., Ortega, F., Mocho, P., & Sanz, J. L. (2016). Femoral variability in two titanosaur taxa from Lo Hueco (Cuenca, Spain): Insights for iberoarmorican titanosaur diversity assessment. In F. Torcida, I. C. Jose, P. Huerta, & X. Pereda-Suberbiola (Eds.), *VII international symposium about dinosaurs palaeontology and their environment* (pp. 107–108). Salas de los Infantes: Colectivo Arqueológico y Paleontológico de Salas.

Páramo, A., Ortega, F., & Sanz, J. L. (2017b). Comparison Between Classification Methods for Isolated Appendicular Titanosaur Bones. In *15th annual meeting of the European Association of Vertebrate Paleontologists. Zitteliana*, 91 (p. 69).

Páramo, A., Ortega, F. & Sanz, J.L. (2019). Morphological disparity and niche exploitation in two Titanosaur forms from the Campanian–Maastrichtian of Lo Hueco (Cuenca, Spain). In *XVII annual meeting of the European Association of Vertebrate Palaeontology.*

Pereda, X., Astibia, H., Murelaga, X., Elorza, J. J., & Gómez-Alday, J. J. (2000). Taphonomy of the Late Cretaceous dinosaur-bearing beds of the Laño Quarry (Iberian Peninsula). *Palaeogeography Palaeoclimatology Palaeoecology, 157*(3–4), 247–275.

Pereda, X., Corral, J. C., Astibia, H., Badiola, A., Bardet, N., Berreteaga, A., et al. (2015). Continental and marine vertebrate assemblages from the Late Cretaceous of the Laño Quarry (Basque-Cantabrian Region, Iberian Peninsula): An update. *Journal of Iberian Geology, 41*(1), 101–124.

Piechowski, R., & Tałanda, M. (2020). The locomotor musculature and posture of the early dinosauriform *Silesaurus opolensis* provides a new look into the evolution of Dinosauromorpha. *Journal of Anatomy*. https://doi.org/10.1111/joa.13155.

Poropat, S. F., Mannion, P. D., Upchurch, P., Hocknull, S. A., Kear, B. P., Kundrát, M., et al. (2016). New Australian sauropods shed light on Cretaceous dinosaur palaeobiogeography. *Scientific Reports, 6*(April), 1–12.

Powell, J. E. (1992). Osteología de Saltasaurus loricatus (Sauropoda–Titanosauridae) del Cretácico Superior del noroeste argentino.

In J. L. Sanz & A. D. Buscalioni (Eds.), *Los Dinosaurios y Su Entorno Biotico Actas del Segundo Curso de Paleontologia in Cuenca (Vol 4)* (pp. 166–229). Cuenca: Instituto "Juan Valdes.".

Powell, J. E. (2003). Revision of South American titanosaurid dinosaurs: Palaeobiological, palaeobiogeographical and phylogenetic aspects. *Records of the Queen Victoria Museum, 111*, 1–179.

Profico, A., Schlager, S., Valoriani, V., Buzi, C., Melchionna, M., Veneziano, A., et al. (2018). Reproducing the internal and external anatomy of fossil bones: Two new automatic digital tools. *American Journal of Physical Anthropology, 166*(4), 979–986.

Remes, K. (2007). *Evolution of the Pectoral girdle and Forelimb in Sauropodomorpha (Dinosauria, Saurischia): Osteology, myology and fuction*. München: Ludwig-Maximilians-Universität München.

Rohlf, F. J. (1998). On applications of geometric morphometrics to studies of ontogeny and phylogeny. *Systematic Biology, 47*(1), 147–158.

Rohlf, F. J. (1999). Shape statistics: Procrustes superimpositions and tangent spaces. *Journal of Classification*. https://doi.org/10.1007/s003579900054.

Rohlf, F. J. (2000). On the use of shape spaces to compare morphometric methods. *Hystrix*. https://doi.org/10.4404/hystrix-11.1-4134.

Royo-Torres, R. (2009). *El saurópodo de Peñarroya de Tastavins* (1st ed.). Teruel: Instituto de Estudios Turolenses y Fundación Conjunto Paleontológico de Teruel-Dinópolis.

Salgado, J. L., Calvo, J. O., & Coria, R. A. (1995). Relaciones filogenéticas de *Pleurocoelus* Marsh (Sauropoda). In *III Jornadas Argentinas de paleontología de vertebrados* (Vol. 18, pp. 156–157).

Salgado, J. L., Coria, R. A., & Calvo, J. O. (1997). Evolution of the titanosaurid sauropods I: Phylogenetic analysis based on the postcranial evidence. *Ameghiniana, 34*(1), 3–32.

Salgado, L., Apesteguía, S., & Heredia, S. E. (2005). A new specimen of *Neuquensaurus australis*, a Late Cretaceous saltasaurine titanosaur from North Patagonia. *Journal of Vertebrate Paleontology*, *25*(3), 623–634.

Sallam, H. M., Gorscak, E., O'Connor, P. M., El-Dawoudi, I. A., El-Sayed, S., Saber, S., et al. (2018). New Egyptian sauropod reveals Late Cretaceous dinosaur dispersal between Europe and Africa. *Nature Ecology and Evolution, 2*(3), 445–451.

Sanz, J. L., Powell, J. E., Le Loeuff, J., Martínez, R. N., & Pereda Suberbiola, X. (1999). Sauropod remains from the Upper Cretaceous of Laño (north central Spain). Titanosaur phylogenetic relationships. *Estudios Del Museo de Ciencias Naturales de Alava, 14*(1), 235–255.

Schlager, S. (2017). Morpho and Rvcg—shape analysis in R. In G. Zheng, S. Li, & G. Szekely (Eds.), *Statistical shape and deformation analysis* (pp. 217–256). New York: Elsevier.

Schlager, S., Profico, A., Di Vincenzo, F., & Manzi, G. (2018). Retrodeformation of fossil specimens based on 3D bilateral semi-landmarks: Implementation in the R package "Morpho". *PLoS One, 13*(3), e0194073.

Sereno, P. C. (2007). Basal sauropodomorpha: Historical and recent phylogenetic hypotheses, with comments on *Ammosaurus major* (MARSH, 1889). *Special Papers in Palaeontology., 77*, 261–289.

Souter, T., Cornette, R., Pedraza, J., Hutchinson, J. R., & Baylac, M. (2010). Two applications of 3D semi-landmark morphometrics implying different template designs: The theropod pelvis and the shrew skull. *Comptes Rendus Palevol, 9*(6–7), 411–422.

The R Core Team. (2016). *A language and environment for statistical computing*. R Foundation for Statistical Computing, Vienna. https://www.R-project.org/.

Tschopp, E., Mateus, O., & Benson, R. B. J. (2015). A specimen-level phylogenetic analysis and taxonomic revision of Diplodocidae (Dinosauria, Sauropoda). *PeerJ, 3*, e857.

Ullmann, P. V., Bonnan, M. F., & Lacovara, K. J. (2017). Characterizing the evolution of wide-gauge features in stylopodial limb elements of titanosauriform sauropods via geometric morphometrics. *The Anatomical Record, 300*(9), 1618–1635.

Ullmann, P. V., & Lacovara, K. J. (2016). Appendicular osteology of Dreadnoughtus schrani, a giant titanosaurian (Sauropoda, Titanosauria) from the Upper Cretaceous of Patagonia, Argentina. *Journal of Vertebrate Paleontology*. https://doi.org/10.1080/02724634.2016.1225303.

Upchurch, P., Barrett, P. M., & Dodson, P. (2004). Sauropoda. In D. B. Weishampel, P. Dodson, & H. Osmólska (Eds.), *The dinosauria* (2nd ed., pp. 259–322). Berkeley: University of California Press.

Upchurch, P., Barrett, P. M., & Galton, P. M. (2007). A phylogenetic analysis of basal sauropodomorph relationships: Implications for the origin of Sauropod dinosaurs. *Special Papers in Palaeontology, 77*, 57–90.

Upchurch, P., Mannion, P. D., & Taylor, M. P. (2015). The anatomy and phylogenetic relationships of "*Pelorosaurus*" *becklesii* (Neosauropoda, Macronaria) from the Early Cretaceous of England. *PLoS One, 10*(6), e0125819.

van Buren, C. S., & Bonnan, M. F. (2013). Forearm posture and mobility in quadrupedal dinosaurs. *PLoS One, 8*(9), e74842.

Venables, W. N., & Ripley, B. D. (2002). *Modern applied statistics with S* (4th ed.). Berlin: Springer.

Vidal, D., & Díez Díaz, V. (2017). Reconstructing hypothetical sauropod tails by means of 3D digitization: Lirainosaurus astibiae as case study. *Journal of Iberian Geology, 43*(2), 293–305.

Vila, B., Galobart, À., Canudo, J. I., Le Loeuff, J., Dinarès-Turell, J., Riera, V., et al. (2012). The diversity of sauropod dinosaurs and their first taxonomic succession from the latest Cretaceous of southwestern Europe: Clues to demise and extinction. *Palaeogeography, Palaeoclimatology, Palaeoecology, 350–352*, 19–38.

Voegele, K. K., Ullmann, P. V., Lamanna, M. C., & Lacovara, K. J. (2020). Appendicular myological reconstruction of the forelimb of the giant titanosaurian sauropod dinosaur *Dreadnoughtus schrani*. *Journal of Anatomy*. https://doi.org/10.1111/joa.13176.

Whitlock, J. A. (2011). A phylogenetic analysis of Diplodocoidea (Saurischia: Sauropoda). *Zoological Journal of the Linnean Society*. https://doi.org/10.1111/j.1096-3642.2010.00665.x.

Wiley, D. F., Amenta, N., Alcantara, D. A., Ghosh, D., Kil, Y. J., Delson, E., & Hamann, B. (2005). Evolutionary morphing. In *Proceedings of IEEE visualization 2005* (pp. 1–8). Minneapolis.

Wilson, J. A. (2002). Sauropod dinosaur phylogeny: Critique and cladistic analysis. *Zoological Journal of the Linnean Society, 136*, 215–275.

Wilson, J. A., & Carrano, M. T. (1999). Titanosaurs and the Origin of "wide-gauge" trackways: A biomechanical and systematic perspective on sauropod locomotion. *Paleobiology, 25*(2), 252–267.

Wilson, J. A., & Sereno, P. C. (1998). Early evolution and high-level phylogeny of sauropod dinosaurs. *Journal of Vertebrate Paleontology, 18*(2), 1–68.

Wilson, J. A., & Upchurch, P. (2003). A revision of *Titanosaurus* Lydekker (Dinosauria—Sauropoda), the first dinosaur genus with a "Gondwanan" distribution. *Journal of Systematic Palaeontology, 1*(3), 125–160.

Young, C. C., & Chao, S. C. (1972). *Mamenchisaurus hochuaensis* sp. nov. *Memoirs of the Institute of Vertebrate Paleontology and Paleoanthropology Academia Sinica, 8*, 1–30.

Zelditch, M. L., Swiderski, D. L., & Sheets, H. D. (2012). *Geometric morphometrics for biologists* (2nd ed.). Oxford: Elsevier.